# Experimental Model for Predicting Cutting Forces in Machining Carbon Fiber Reinforced Polymer Composites

by

Amirali Ahmadian
B.Sc., Iran University of Science and Technology, 2013

A Thesis Submitted in Partial Fulfillment
of the Requirements for the Degree of

MASTER OF APPLIED SCIENCE

in the Department of Mechanical Engineering

# Supervisory Committee

Experimental Model for Predicting Cutting Forces in Machining Carbon Fiber Reinforced Polymer Composites

by

Amirali Ahmadian
B.Sc., Iran University of Science and Technology, 2013

**Supervisory Committee**

Dr. Keivan Ahmadi, (Department of Mechanical Engineering)
**Supervisor**

Dr. Afzal Suleman, (Department of Mechanical Engineering)
**Departmental Member**

# Abstract

**Supervisory Committee**
Dr. Keivan Ahmadi, (Department of Mechanical Engineering)
**Supervisor**
Dr. Afzal Suleman, (Department of Mechanical Engineering)
**Departmental Member**

The demand for materials with high mechanical performances such as Carbon Fiber Reinforced Plastics (CFRP) is increasing. However, there are major challenges in machining CFRP as it involves delamination, fiber pullouts, and extreme cutting tool wear. Analysis of chip formation mechanisms and prediction of associated cutting forces in CFRP machining enables one to address these challenges. This study proposes a mechanistic cutting force model for milling operations of the CFRP workpiece, considering its non-homogeneity and anisotropy, by taking into account variations of fiber cutting angle during machining. A mechanistic model of cutting force constants is obtained from a number of experimentally measured unidirectional CFRP milling forces. The obtained mechanistic force model predictions are verified against experimentally measured milling forces with arbitrary tool path indicating the accuracy of the proposed mechanistic model in predicting cutting forces. The proposed mechanistic cutting force model is capable of being integrated into the manufacturing process to allow optimized machining of quality certified CFRP work-pieces.

# Table of Contents

# List of Tables

# List of Figures

# Acknowledgments

I would like to thank:

**Hamid Ahmadian, Mojdeh Ghodsi, and Navid Ahmadian** for all the love, support, constant encouragements and the amazing chances they have given me over the years.

**Afzal Suleman** for his encouragement during my master's studies. I have been lucky to have a committee member who cared so much about my work, and it was an honor for me to learn from your amazing personality.

**Canadian Network for Research and Innovation in Machining Technology (CANRIMT)** for the financial support and the opportunity to work on this project.

**Industrial Technology Research Institute (ITRI), Taiwan** for the opportunity to do an amazing internship in Taiwan and providing the test equipment and technical assistance during this research.

# Nomenclature

| | |
|---|---|
| CFRP | Carbon Fiber Reinforced Polymer/Plastic |
| UD | Uni-Directional |
| MD | Multi-Directional |
| EHM | Equivalent Homogenous Material |
| FEM | Finite Element Modelling |
| FRP | Fiber Reinforced Polymer/Plastic |
| GFRP | Glass-Fiber Reinforced Polymer/Plastic |
| $\theta$ | Fiber Orientation Angle |
| $\beta$ | Fiber Cutting Angle |
| $\varphi$ | Tool Immersion Angle |
| $\varphi_{st}$ | Initial Value of Tool Immersion Angle |
| $\varphi_{ex}$ | End Value of Tool Immersion Angle |
| $c$ | Chip Load |
| $h$ | Instantaneous Chip Thickness |
| $g$ | Control Function |
| $M$ | Harmonic number |
| $D$ | Tool Diameter |
| $F_t, F_r$ | Tangential Force, Radial Force |
| $F_x, F_y$ | Cutting Force in x-direction, Cutting Force in y-direction |
| $K_{tc}$ | Cutting Force Coefficient in Tangential Direction |

| | |
|---|---|
| $K_{rc}$ | Cutting Force Coefficient in Radial Direction |
| $K_{te}$ | Rubbing Force Coefficient in Tangential Direction |
| $K_{re}$ | Rubbing Force Coefficient in Radial Direction |
| $a$ | Edge Contact Length |
| $N$ | Number of Flutes |

# Chapter 1
# Overview and Research Objective

## 1.1. Introduction

Carbon Fiber Reinforced Polymers (CFRP) are a class of high strength, lightweight, and resistant to corrosion fiber reinforced polymer. The growing demand for efficiency requires lightweight industrial structures which have caused the steadily increasing use of CFRP in the industry, especially in the aerospace. Metals and other materials that cannot keep pace with the CFRP performance are being replaced by them. While usage of aluminum alloys has led to less manufacturing challenges, the CFRP machining process encounters with difficulties in surface finish quality and tool lifetime. Also, anisotropic and inhomogeneous material properties cause problems during machining such as extremely strong tool wear and the composite material tends to damages, such as delamination formation.

CFRP parts are fabricated near net shape but post machining operations such as drilling and trimming are needed to assure part dimensions are within the defined tolerances and giving the final shape. Extensive research has been conducted on drilling and turning operations of composites but the number of studies done on milling of CFRPs is quite limited.

The development of better manufacturing and post-treatment techniques for CFRPs are improving their use from an economic point of view. Although non-conventional machining processes are available and solve some of the issues related to CFRP machining, conventional machining processes are highly preferred for reasons of cost and time. However, extensive studies on machining process optimization are required in order to achieve adequate cutting quality results. Therefore, further study on machining forces in the milling of composites is required and is considered in this research work.

## 1.2. Research Objectives

There have been many studies on predicting cutting forces in metal cutting. Mechanistic force modeling is among the most efficient methods and is employed for simulating milling operations. In this method, constant parameters of the tool geometry-workpiece material pair are identified by conducting milling experiments. Due to the anisotropic nature of CFRP's, the chip formation mechanics is different from metals and there are concerns regarding phenomena such as fiber pull-outs, delamination, and etc. which are not present in metal cutting. The abrasive properties of CRFP impose high wear in the tool and significantly change the cutting forces during machining. Other concerns regarding CFRP machining are the generated dust which causes skin irritation and damages the lungs and respiratory system.

The cutting forces in CFRP machining are functions of fiber and matrix properties, their relative volume, and the fiber orientation. Experimental works conducted on the cutting of unidirectional CFRP indicates the resultant surface quality is a function of fiber orientation. In CFRP machining it is observed the surface is destroyed and cracks are formed during machining perpendicular to the fibers, while machining in parallel to the fibers produces smoother surfaces [1].

Very few studies have been conducted for cutting force modeling in CFRP milling operations. Finite element, analytical, and experimental techniques are used for simulating chip formation in cutting CFRPs. The CFRP chip is formed by fracture; shear or both mechanisms are involved, governed by the fiber orientation and tool geometry.

This research study proposes a mechanistic cutting force model based on unidirectional CFRPs milling experiments. The radial and tangential cutting force coefficients are functions of fiber cutting angle. The present study defines the cutting force coefficients as periodic functions of fiber cutting angle. These periodic functions are expanded using Fourier series and are identified from a number of UD CFRP experimental results. Identified cutting force coefficients enable one to predict cutting forces in any complex milling path as required in many industrial applications.

## 1.3. Thesis Layout

The research study conducted in this thesis and the developed mechanistic cutting force model of CFRP in milling is presented in six chapters. Chapter 2 provides a literature review on chip formation and milling force modeling for CFRP. Chapters 3 and 4 consider the mechanistic models of cutting forces in metals and CFRPs. As bases for defining cutting force in CFRP are originated in metal cutting, chapter 3 defines the fundamentals of metal cutting forces. Also in this chapter, the cutting force coefficients are identified from experimentally measured machining forces. Chapter 4 describes mechanistic cutting force models in CFRP machining and it proposes further developments in the existing models by employing a Fourier series expansion in describing the cutting force coefficients. Chapter 5 introduces the test setup and UD-CFRP experiments conducted to identify the cutting force coefficients. Also, verification of the proposed model in predicting cutting forces in UD and an arbitrary tool path in CFRP milling is conducted in Chapter 5. Finally, chapter 6 provides analysis and discussions of results obtained in the development of the CFRP milling force mechanistic model.

# Chapter 2
# Machining of Fiber Reinforced Polymers: A Literature Review

Carbon fiber reinforced polymers (CFRPs) allow superior mechanical properties that enable to enhance higher functional performance. Due to this advantageous material property compared to other material, CFRPs are widely used in the industry. Post machining of CFRPs is an essential procedure that assures the manufactured components meet their dimensional tolerances, surface quality, and other requirements. This process is one of the main challenges in using these materials for different applications due to the highly nonlinear, inhomogeneous, and abrasive nature of CFRPs. In this chapter, a literature review on the machining of CFRPs is given with a focus on the main issues including tool wear, delamination, and burr formation.

## 2.1. Fiber Reinforced Polymers

Composites are defined as materials with two or more different basic components. The purpose of producing composites is to reach better properties by employing the advantages of each component individually. Fiber reinforced composites involve fibrous materials which improve the strength, stiffness and thermo-mechanical behavior of the component. Basically, FRPs consist of fibers embedded in polymer matrices. A fibrous material has a much higher strength in the fiber direction compared to other directions. The matrices are responsible for the shaping of the part and guidance of the loads between the fibers, as well as protecting the fibers [2].

CFRPs are extremely strong and light-weighted fiber reinforced polymers build with carbon fibers. The polymer is often epoxy, but other polymers, such as polyester are used as well. CFRPs offer a very high strength-to-weight ratio, high modulus-to-weight ratio, high damping capacity, good dimensional stability, excellent damage tolerance, and good corrosion and fatigue resistance [3]. Figure 2-1 presents a composite part life cycle. As can be found from the figure, the part machining is usually at the final stage of the manufacturing process and due to this matter, it makes it more important and critical.

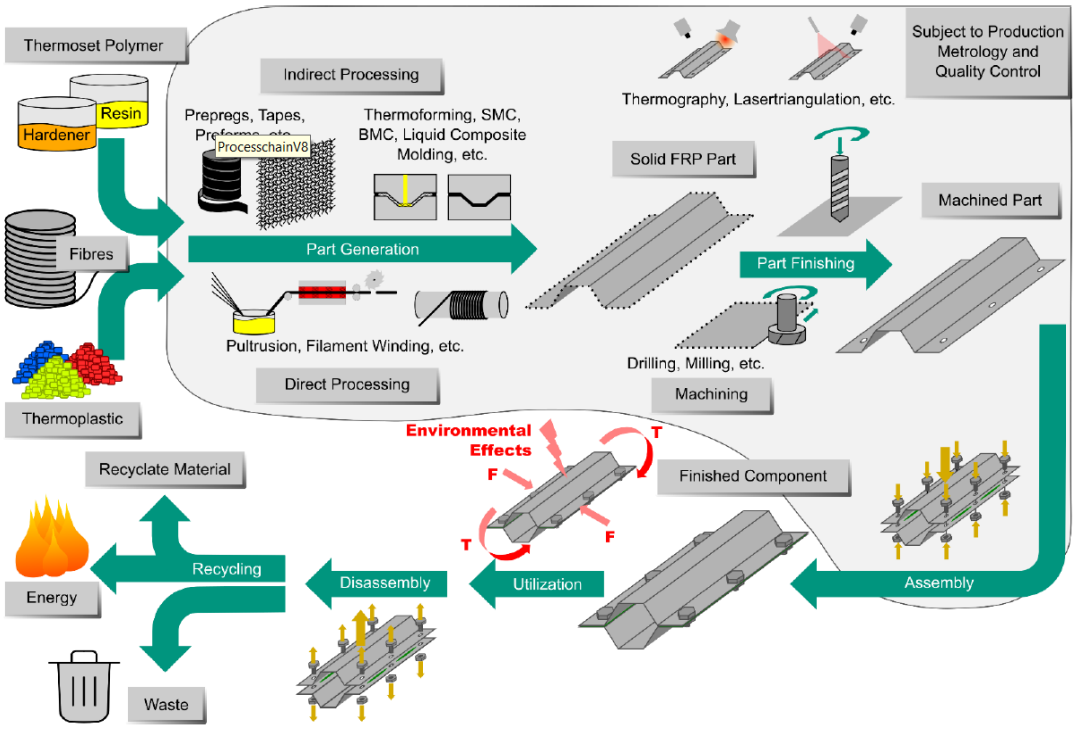


**Figure 2-1: Product Life Cycle for Composite Materials Parts Manufacturing** [2]

## 2.2. FRP Composite Material Machining

The theory underlying chip formation in composite materials is different from the ones defined for metal cutting which is due to the significant material property difference. Also, the literature available on composite machining and post-treatment is limited compared to metals [4]. In this study, the literature available on composite material machining is first reviewed for orthogonal cutting operations, which helps with understanding the chip formation process, and then studies conducted on composite milling operations are presented.

### 2.2.1. Orthogonal Cutting

In order to study the influence of cutting parameters and achieve adequate machining quality, it is required to investigate cutting forces generated during simple machining operations [5]. Orthogonal cutting is one of the basic machining operations that can help one understand the phenomena underlying chip formation in composites specially CFRP's. In orthogonal cutting, the tool edge is perpendicular to the direction of the

cutting speed vector. Orthogonal cutting experiments provide the opportunity to apply constant cutting speed, chip thickness, and fiber orientation which is the reason why many researchers have chosen this process for studying.

Chip formation mechanism and forces generated while machining CFRPs are highly dependent on the fiber orientation [6]. Also, the material is removed through a brittle failure and rupture rather than shearing which is observed in metals [7]. Different fiber orientations in CFRPs initiate different material removal process. This is the reason why there is particular attention to this parameter in composite material machining [8].

In [9] and [10] orthogonal cutting experiments of both unidirectional and multidirectional carbon fiber reinforced polymers are performed at different fiber orientations (Figure 2-2). During these experiments, the cutting forces, chip generation, and surface quality were monitored. It was found that the failure mode in chip generation is primarily dependent on fiber orientation and other machining conditions such as cutting tool rake angle have a secondary effect.

In [11] the importance of fiber orientation angle during orthogonal machining of unidirectional fiber reinforced polymers is also noticed which determines the surface integrity of the machined part. Authors found out that there are three distinct deformation zones for fiber orientation angles lower than $90^o$ which is bouncing, pressing, and chipping. For fiber orientations higher than $90^o$, fiber bending became more considerable. This study also investigates the influence of cutting tool rake angle and the cure condition during the FRP part production. The rake angle only affects machined surface quality and better surface roughness will be achieved with rake angles lower than $20^o$. Also, the cure degree had no impact on the surface quality and slightly affected the cutting forces. In [12], the surface roughness of machined UD and MD CFRP workpiece were measured using electron microscopy scanning. It was found that the surface quality and profile are extremely influenced by the fiber orientation and measurement direction.

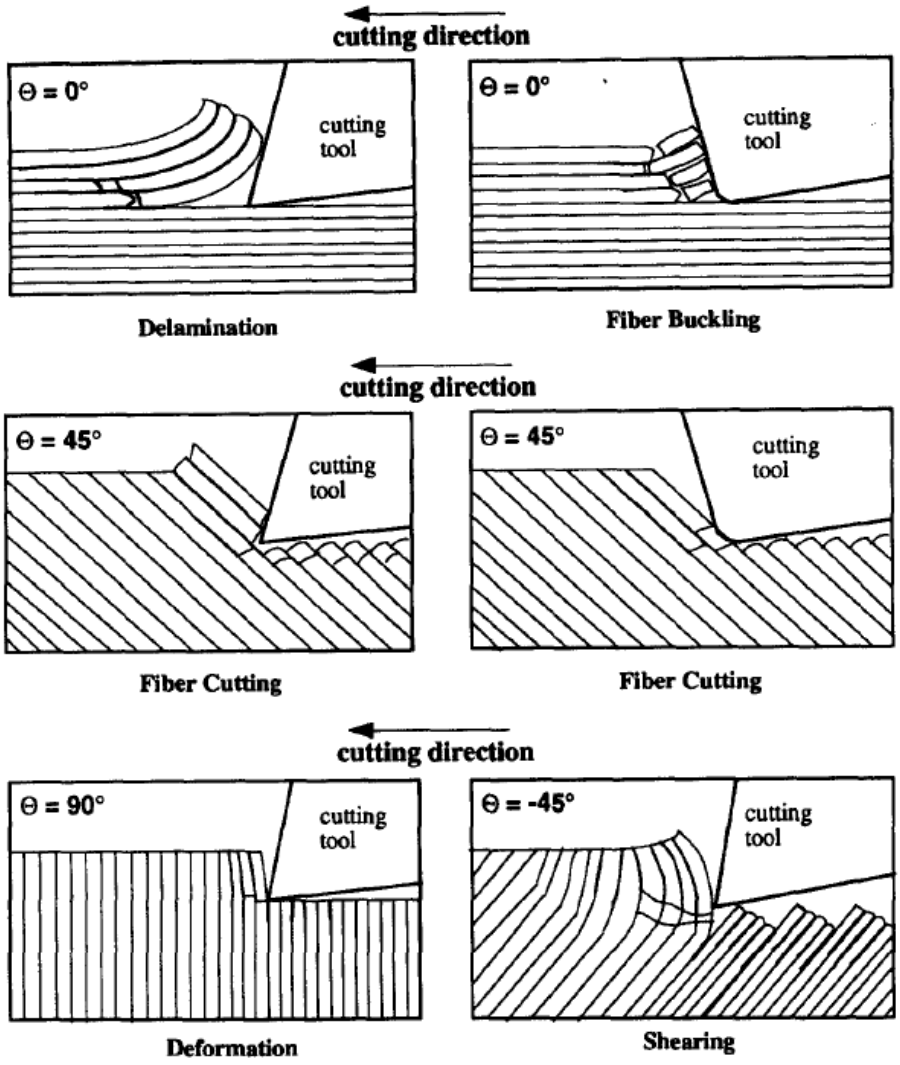


**Figure 2-2: Cutting mechanisms in CFRP orthogonal machining** [9]

Several researchers have performed finite element modeling for simulating the chip formation process in FRP composites. The literature available includes numerical studies with different damage and constitutive material model, tool geometry and element type. There are two major approaches for simulating FRP composites orthogonal cutting which includes Micro-Mechanical and Macro-Mechanical approach. In the Micro-Mechanical approach, fiber and matrix are modeled separately and the interaction between them needs to be defined. This approach leads to the most accurate results but it is time consuming due to the large computation required. In the Macro-Mechanical approach, an Equivalent Homogenous Material (EHM) with orthotropic properties is employed for the

composite workpiece. This assumption makes the model and the computation simple compared to the former approach and also presents reliable results [13].

In [14], a 3-dimensional finite element cutting simulation is presented for a composite cell. The cell consists of $90^o$ fiber orientation and the matrix with a perfect bonding between the two phases. An adaptive meshing was employed which improved the simulated cutting forces comparing to a non-adaptive model. This was an efficient method to accomplish smooth material removal. In [15], a 2-D finite element model with equivalent homogeneous material is developed in order to predict the cutting forces in FRP composites. The cutting forces were related to the fiber orientation and compared with the experimental data.

The effect of tool geometry on cutting forces, sub-surface damage and stresses developed in the tool are investigated in [16]. This study was carried out by developing a finite element model simulating chip formation in edge trimming of unidirectional FRP's. The cutting tool in [16] was modeled both as a rigid and deformable body in individual simulations.

### 2.2.2. Milling

Milling processes are widely used for fiber reinforced composites as a post-treatment operation in order to produce high-quality surfaces and keep dimensions within the defined tolerances [17]. Delamination and burrs occurred during CFRP machining are the major issues which limit the manufacturing process. Many attempts have been conducted for avoiding delamination and burr formation. Accurate prediction of cutting forces can help to perform process parameter optimization and avoid defects mentioned earlier [18]. It has also been shown that applying certain tool paths can lead to less delamination and damage evolution [19].

Researchers have investigated CFRP milling with high feedrates to identify the influence it has on machining parameters. In [20], for cutting speeds up to 1500 mm/min, the cutting forces and tool wear, and carbon dust generated during machining was determined. Ref. [21] found that by applying high cutting speeds in CFRP machining, the

chip formation process changes. Also increasing the cutting speed reduces the cutting forces which can be used for extending the cutting tool operating life. In [22], vibration assisted milling with a maximum frequency of 30 Hz was studied. A unidirectional CFRP workpiece with a thickness of 1.5 mm was used during this research. Influence of the tool and the fiber orientation angle on delamination and surface finish was investigated. It was found that the tool and the fiber orientation angle have an important impact on delamination formation. With a special solid carbide tool, delamination was reduced compared to conventional milling, independently of fiber orientation angle.

Ref. [23] investigated machining CFRPs during slot milling with the focus being on the process of contour milling. It was observed that the occurrence of delamination is closely related to tool wear and top layer fiber cutting angle. Top layer delamination initiation is distinguished from its propagation. Both mechanisms occur at different ranges of the fiber cutting angle as shown in Figure 2-3. Top layer delamination results from bending of fiber within the laminate plane or perpendicular to it, based on the fiber cutting angle [24].

In [25], a helical milling process was applied to FRP components. The work compared axial drilling with a helical milling process from both final product quality and processing time point of view. The cutting tool didn’t follow a helical path whilst moving in an axial direction but rather followed a step-wise trajectory. Workpiece quality, fiber pull-out, and fiber protrusion and their dependency on process and tool parameters were analyzed. It was found that the helical milling process produces higher bore hole qualities but also increased the processing time.

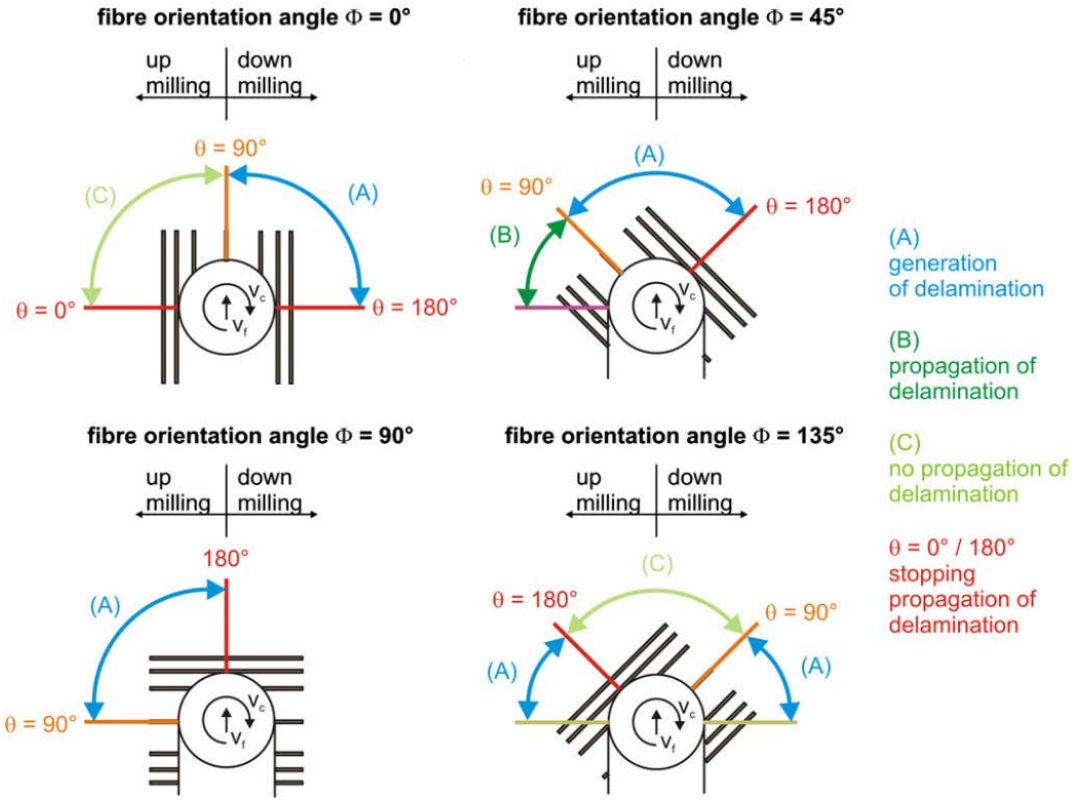


**Figure 2-3: Occurrence of delamination in the milling of CFRP composite** [23]

Conventional tool designs don't consider the different machining behavior of fiber reinforced polymers compared to metals. Tool materials for FRP milling need to attain high hardness and thermal conductivity. Ref. [26] introduces fundamental tool-geometry analyses in cutting unidirectional CFRP material. Extensive experiment series is performed and based on different tool geometries and fiber-orientations, process parameters such as cutting forces, tool wear, workpiece damages, and delamination are evaluated. Tool life of uncoated and diamond coated carbide end mills during CFRP milling was also investigated.

Ref. [27] proposes a mechanistic cutting force model for milling CFRPs. This model is based on experimentally collected cutting force data. The authors used UD laminates and measured the forces using a rotating type dynamometer. Cutting force coefficients in radial and tangential directions were calculated as a function of fiber cutting angle. The mechanistic model was capable of predicting cutting forces during milling of multidirectional CFRP laminates as well.

In [28], 2D and 3D finite element models were presented for simulating the milling process of CFRP with different levels of tool wear. Models were validated by edge trimming experiments on a unidirectional laminate using a three flute milling tool. In this study Hashin damage material model was introduced into the finite element simulation model. A percentage difference of 10% and 5% was obtained for the 3D model for the feed and normal to feed forces respectively. For the 2D model (Figure 2-4), the percentage difference was 9% and 50%. Also, tool wear was found to have a significant effect on the measured cutting forces.

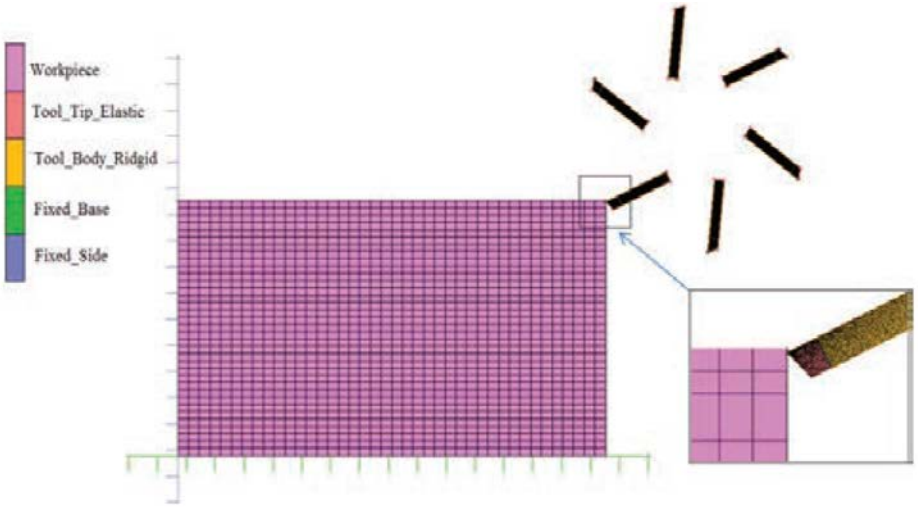


**Figure 2-4: Finite element model for CFRP edge trimming** [28]

## 2.3. Conclusion

It is observed the current studies in the literature are focused on providing efficient models to predict machining forces in CFRPs. This is to the demand of industries dealing with CFRP machining processes to reduce the tool wear and increase the workpiece surface finish quality. This thesis considers modeling cutting forces in milling processes of CFRPs and provides a mechanistic cutting force model to predict the machining forces. The provided model in the present study may be used to accurately determine the milling forces of a CFRP workpiece machining. Hence by selecting the optimum machining parameters based on the provided model, it is possible to reduce the cutting forces and to improve the workpiece surface finish quality.

# Chapter 3
# Mechanistic Modeling of Cutting Forces for Metals

This chapter describes a commonly used mechanistic model which defines the relations between chip geometry in milling and resulting cutting forces for isotropic materials such as metals. It is shown that this relationship is a linear one and its coefficients are obtained using experimentally measured cutting forces.

## 3.1. Mechanics of Milling Processes

In milling operations, as shown in Figure 3-1, the chip is formed when the cutting edges of the tool are engaged with the workpiece. The contact between tool and workpiece occurs when the tool immersion angle is between $\phi_{st}$ and $\phi_{ex}$. These angles depend on the tool diameter and its radial immersion.

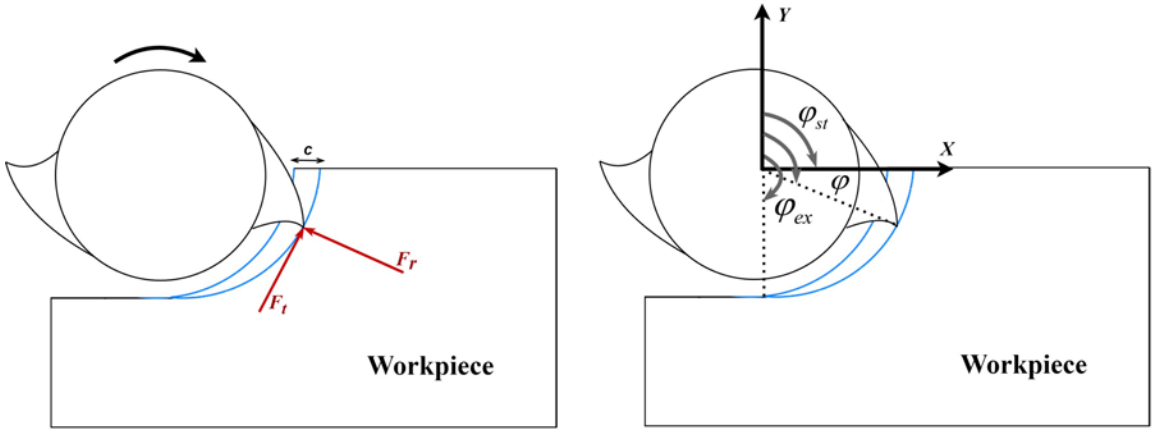


**Figure 3-1: Chip formation geometry and fixed reference frame**

The thickness of the chip, *h*, that is removed by each flute varies periodically with the tool rotation angle and is expressed as

$$h(\phi) = c \sin\phi, \quad \phi_{st} \le \phi \le \phi_{ex}, \tag{3.1}$$

where $c$ is the feed per revolution per tooth and $\phi$ is immersion angle.

For simplicity of the formulation, the tool helix angle, and its edge radius are considered zero. In a mechanistic cutting force model, the cutting forces in tangential and radial directions on each flute are expressed as linear functions of the instantaneous uncut chip thickness [29]

$$F_t(\phi) = K_{tc} a h(\phi) + K_{te} a \tag{3.2}$$

$$F_r(\phi) = K_{rc} a h(\phi) + K_{re} a \tag{3.3}$$

where $a$ is the axial depth of cut, $K_{tc}$ and $K_{rc}$ are cutting shear force coefficients in tangential and radial directions contributed by shearing action, $K_{te}$ and $K_{re}$ are edge force coefficients. A similar expression is used to define the axial force in milling operations. The axial cutting force depends on tool helix angle and in this study, it is considered negligible as the tool helix angle is small.

Feed and normal components of the cutting forces applied to the tool are

$$F_x(\phi) = -F_t \cos\phi - F_r \sin\phi \tag{3.4}$$

$$F_y(\phi) = F_t \sin\phi - F_r \cos\phi \tag{3.5}$$

The overall forces are obtained by projection of the radial and tangential forces from each flute to the machining feed and normal directions. The tool is assumed to have $N$ flutes indexed as $j = 1..N$ each with the cutter entry and exit angles $\phi_{st} \le \phi_j \le \phi_{ex}$ and then summing the forces from all the flutes

$$F_x = \sum_{j=1}^{N} F_{xj}(\phi_j) \tag{3.6}$$

$$F_y = \sum_{j=1}^{N} F_{yj}(\phi_j) \tag{3.7}$$

The uniform pitch angle between consecutive flutes is $\phi_p = \frac{2\pi}{N}$ assuming that the first flute ( $j = 1$ ) is started from the Y-axis as shown in Figure 3-1.

Employing Equations (3.1-3.7), one may determine the milling forces in the machining process. In the determination of these force, two set of input data are required, namely the geometric information as defined in Figure 3-1 and the cutting force coefficients. While the geometric information is readily available in machining the cutting force coefficients are identified experimentally as described in the followings.

## 3.2. Identification of Specific Force Coefficients

One approach in the determination of applied forces on a cutting tool is to calculate friction and pressure loads on its rake face. In a cutting tool with a complex cutting edge, the load is a function of a vast number of geometric parameters including shearing angle, shearing strength, and friction coefficient. The procedures to determine these parameters requires creating a time-consuming orthogonal cutting database which may not be possible. An alternative approach is identifying the cutting forces using experimentally measured data. The following introduces two methods of identifying cutting force coefficients defined in Eqns. (3.2-3) using measured cutting forces.

### 3.2.1. Instantaneous Force Method

One may measure the cutting forces in a milling operation using a dynamometer. The machining operation is performed with a specified tool, workpiece, chip load, depth of cut, and immersion angles. Geometrical parameters of the machining operation are known and to define the cutting forces using mechanistic model described in section 3.1 one requires the cutting constants $K_{tc}$, $K_{rc}$, $K_{te}$ and $K_{re}$ . These constants are obtained by curve fitting the model defined in Eqns. (3.2-3) to the experimentally measured cutting forces via an optimization procedure [30]. In the optimization problem, the objective function is defined as the difference between mechanistic model force predictions and the measured forces as shown in Figure 3-2. The design variables are the cutting constants and inequality constraints of,

$$K_{tc} > 0., \tag{3.8a}$$

$$K_{rc} > 0., \tag{3.8b}$$

$$K_{te} \geq 0., \tag{3.8c}$$

$$K_{re} \geq 0., \tag{3.8d}$$

are applied to ensure positivity of the identified cutting coefficients.

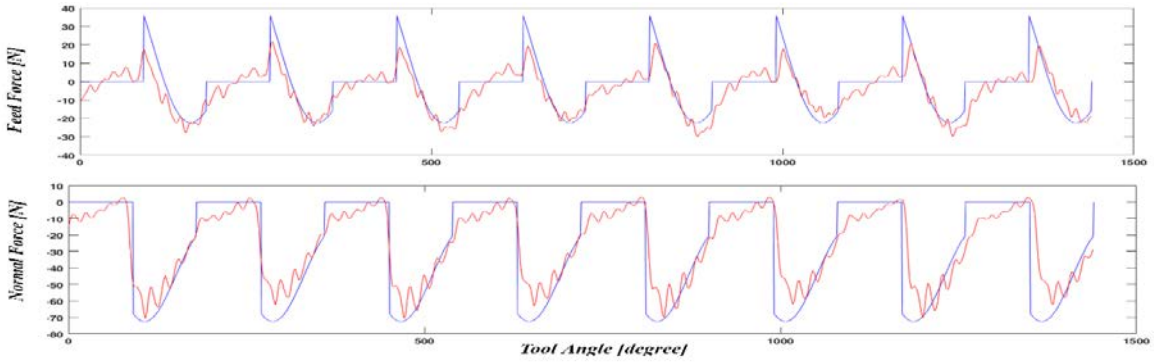


**Figure 3-2: Measured (red) and predicted (blue) cutting forces**

The measured forces contain harmonic components that are not represented in the mechanistic model as observed in Figure 3-2. The harmonic components are mainly due to vibrations and runout that cause bias errors in the determination of cutting constants. Averaging of cutting forces over time cancels the effects of these harmonic components. This motivates the use of average force strategy in cutting constants identification which is described in the following section.

### 3.2.2. Average Force Method

In this method, a small series of milling experiments with different feed rates are conducted at a constant axial and radial depth of cut. The average cutting forces per tooth period are calculated by using these measurements and it is assumed that they are the input factors to derive cutting force coefficients. This approach is a standard practice in industry and the detail can be found in Ref. [29].

The illustration of the analytical equation for the average cutting force is

$$\overline{F}_q = \frac{1}{\phi_p}\int_{\phi_{st}}^{\phi_{ex}} F_q(\phi)d\phi,\ q = x, y \tag{3.9}$$

Since the material being removed is constant in one tooth period regardless of the helix angle, the magnitude of the average cutting force is independent of the helix angle. Also, each tooth cuts within its immersion zone. Therefore, in a case of half immersion down milling cutting experiment ($\phi_{st} = \frac{\pi}{2}, \phi_{ex} = \pi$) with a two fluted milling tool and depth of cut *a*, the average force per tooth period can be derived as follows

$$\overline{F}_x = \left(\frac{K_{tc}}{2\pi} - \frac{K_{rc}}{4}\right)ca + \frac{K_{te} - K_{re}}{\pi}a, \tag{3.10a}$$

$$\overline{F}_y = \left(\frac{K_{rc}}{2\pi} + \frac{K_{tc}}{4}\right)ca + \frac{K_{te} + K_{re}}{\pi}a. \tag{3.10b}$$

It can be seen that the average cutting forces are expressed as a linear function of $\boldsymbol{c}$, with slope $K_c$ and offset $K_e$. One may rearrange Eqn. (3.10) in terms of unknown cutting force coefficients and calculate them using the measured average forces

$$\begin{Bmatrix}\overline{F}_x \\ \overline{F}_y\end{Bmatrix} = \begin{bmatrix}\frac{ca}{2\pi} & -\frac{ca}{4} & \frac{a}{\pi} & -\frac{a}{\pi} \\ \frac{ca}{4} & \frac{ca}{2\pi} & \frac{a}{\pi} & \frac{a}{\pi}\end{bmatrix}\begin{Bmatrix}K_{tc} \\ K_{rc} \\ K_{te} \\ K_{re}\end{Bmatrix} \tag{3.11}$$

Two equations are obtained for each measurement with a specified chip load while other machining parameters are kept constant. As there are four unknown cutting constants, and considering measurement errors involved in obtaining the average forces, one requires measuring the cutting forces at least three different chip loads. The equations formed using these experimentally measured average forces are solved using the least squares method to determine the cutting constants.

The following section demonstrates an experimental case study designed to identify cutting constants in a half immersion milling of an aluminum workpiece.

## 3.3. Experimental Case Study

An experimental test set up was arranged to measure the cutting forces during a half immersion end mill machining of an aluminum block. In the followings the measurement setup, measured forces at different cutting speeds, identified cutting coefficients, and results of regenerated forces from the mechanistic model versus measured forces are presented.

### 3.3.1. Measurement Setup

In order to obtain the average cutting force coefficients in milling, a series of half immersion milling experiments were performed on a 3-Axis vertical CNC machine. Maximum spindle speed of the machine is 20000 rpm but the selected speed for performed experiments was 4000rpm. The work-piece material was Al-6061 extruded bar stock with approximate dimensions of 80 mm×80 mm×50 mm. Cutting forces were measured by a 9255 3-component Kistler dynamometer which its accuracy is checked by using two 5Kg calibrating weights as shown in Figure 3-3.

**Figure 3-3: Dynamometer Calibration Check**

The aluminum block was clamped to the dynamometer and sufficient torque was applied to make sure it was rigidly fixed. The measured signals were conditioned and amplified using a 9255C Kistler amplifier. Amplified signals were digitized at 10.24 KHz sampling rate using an NI9234 data acquisition card. Cutpro [31] software was used to store the measured force signals. A schematic of the measurement setup is shown in Figure 3-4.

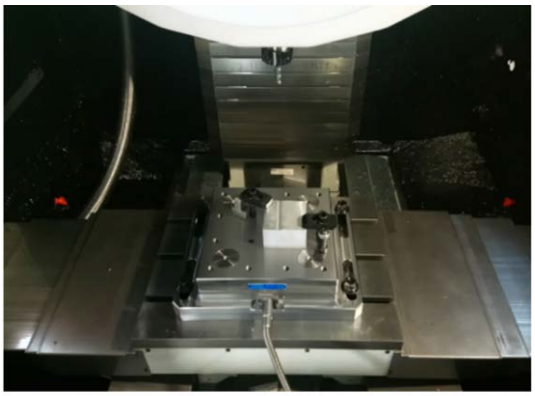

*a) Cutting Station*

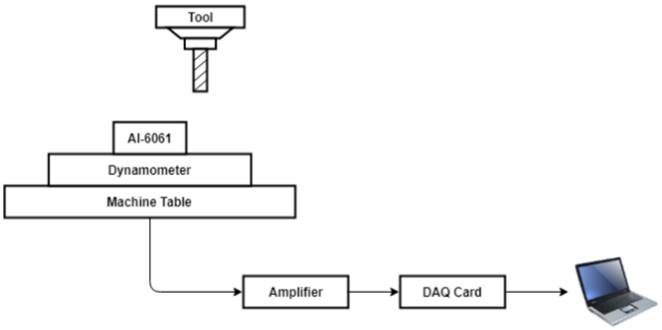


*b) Measurement Setup Scheme*

**Figure 3-4. Al-6061 Cutting Experiment Setup**

A tool of 10mm in diameter is used with 2 flutes and a helix angle of 30 degrees. Table 1 demonstrates further details about the end mill used in this experiment.

**Table 1: HSS1002 Tool Specification**

| Manufacturer | Part Number | Type | Helix Angle | Flutes | Diameter | Full Length |
|---|---|---|---|---|---|---|
| PAN TIGER | HSS1002 | Squared | $30^o$ | 2 | 10mm | 75mm |

Cutting experiments were performed under stable milling conditions with an axial depth of cut of 1mm. Cutting parameters are as follows: spindle speed of 4000 rpm, half immersion down milling, with a series of feed per tooth of 0.05, 0.1, 0.15, 0.2 mm/tooth. During the milling operation, no coolant was used due to the unwanted effects it produced on the measured forces by the dynamometer. Measured forces in feed and normal to feed direction are shown in Figure 3-5 and Figure 3-6.

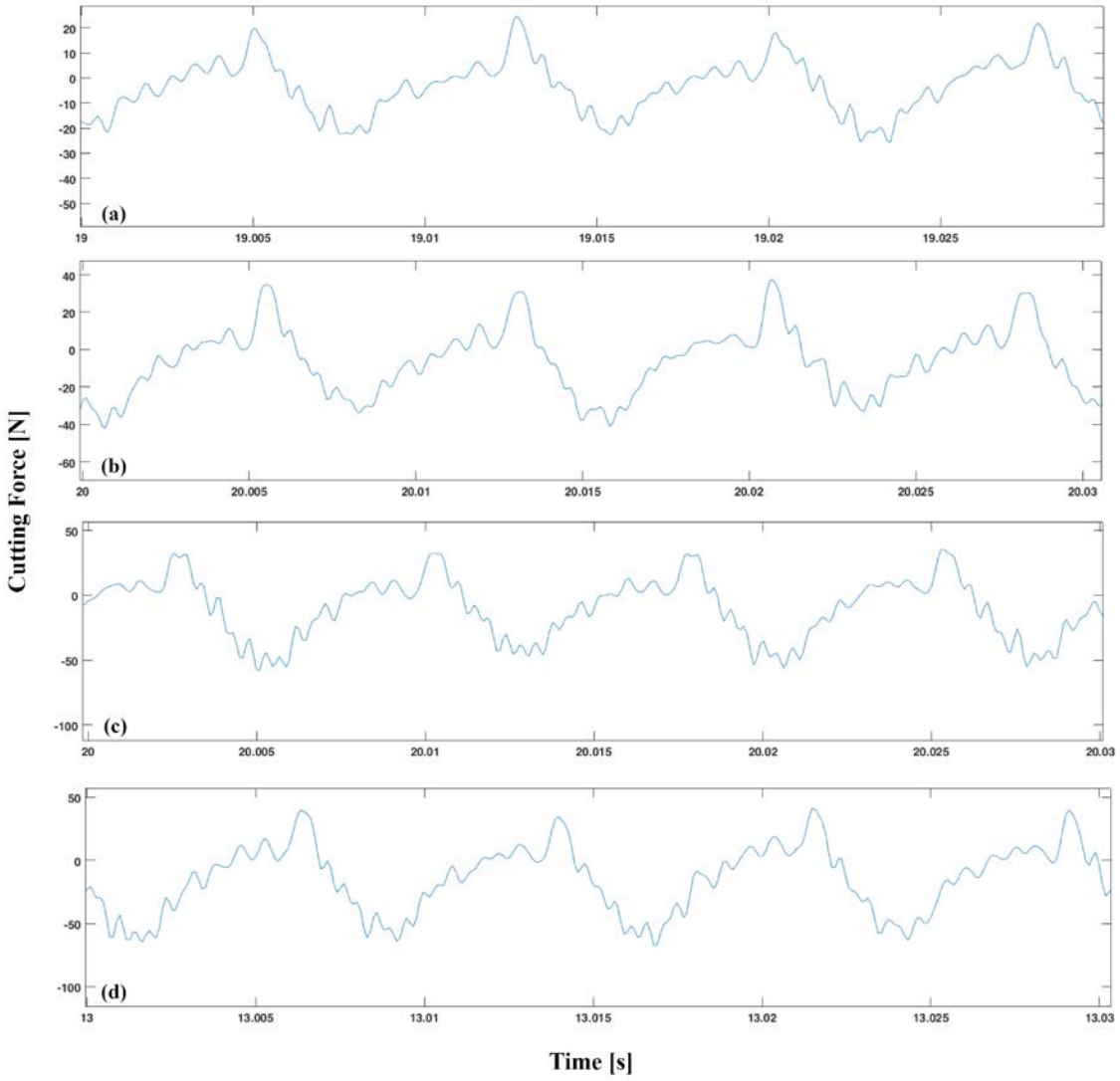


**Figure 3-5: Sample of measured cutting forces for two cutter revolution (a) 400 (b) 800 (c) 1200 (d) 1600 [mm/min] in feed direction**

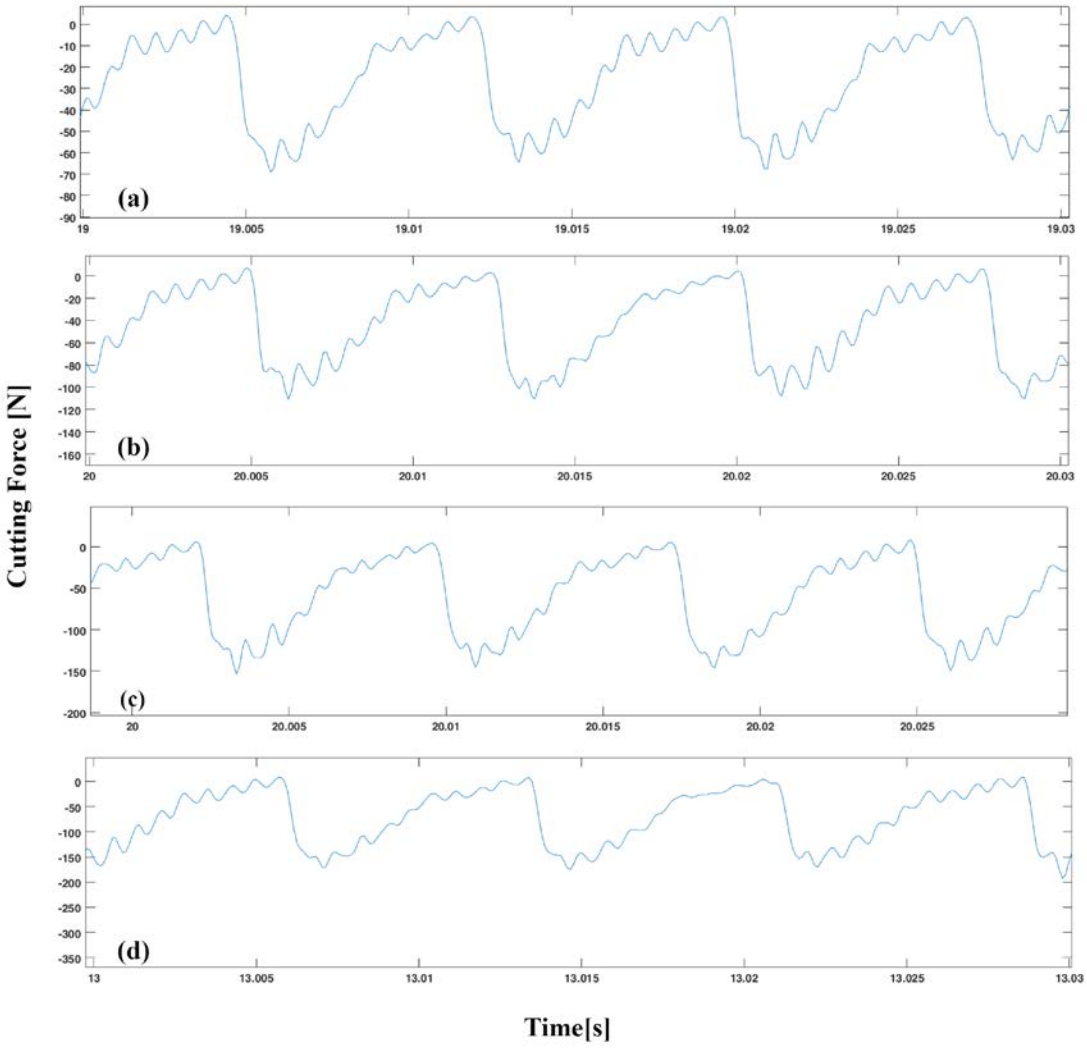


**Figure 3-6: Sample of measured cutting forces for two cutter revolution (a) 400 (b) 800 (c) 1200 (d) 1600 [mm/min] in normal direction**

### 3.2.2. Identifying Cutting Force Coefficients

As mentioned in the previous section, cutting forces data were collected in four different feed rates. In order to identify the cutting force coefficients, the average forces for each feed rate were calculated for the given sampling times. There are several benefits in using the average forces in the identification of cutting force constants. Averaging of the measured forces eliminates the following unwanted effects in the measured forces:

1. The harmonic force components which are mainly originated from spindle vibrations,

2. The tool run-out effects,
3. The effects of tool entering and exiting the workpiece,
4. The tool helix angle effects on cutting forces.

The averages of cutting forces were calculated in different cutting speeds while other machining parameters such as radial and axial depths of cut remained unchanged. The average feed and normal forces are represented in Figure 3-7. These average forces measured at four different feed rates may be used in conjunction with Eqn. (3.11) and form eight equations to identify the cutting constants in the least-squares sense. The measurement errors affect the identified coefficients and these effects may be reduced by increasing the number of measurements at different feed rates.

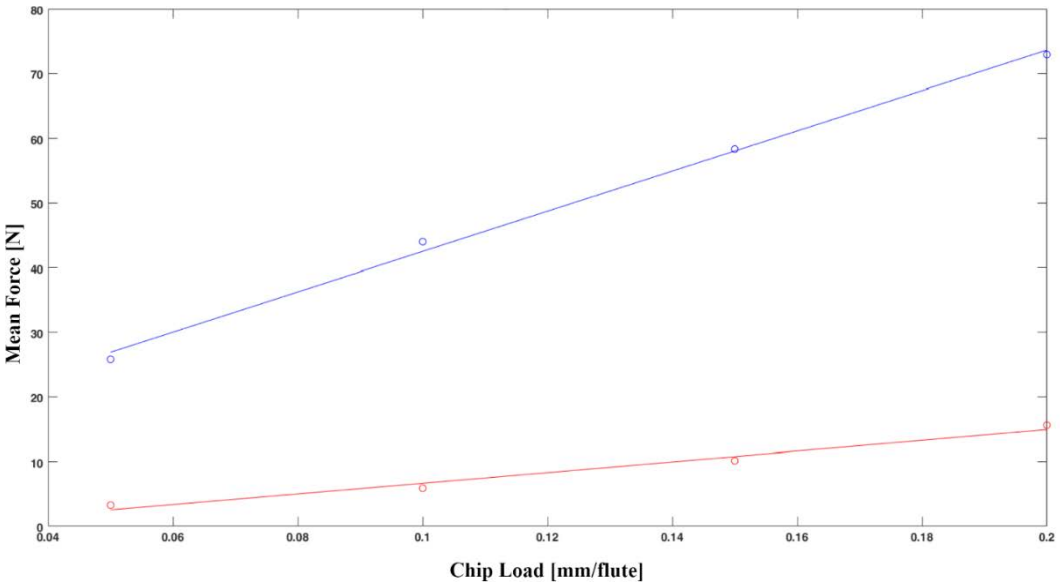


**Figure 3-7: Average force, linear curve fitting result for a half immersion down milling cut at a spindle speed of 4000 rpm (Feed force in blue and normal forces in red)**

In order to remove the measurement errors, one may use the fact that average cutting forces are linear functions of feed rate, i.e.

$$\overline{F}_q = m_q c + b_q, \ q = x, y, \tag{3.12}$$

and fit a line to the measured average forces as shown in Figure 3-7. Relations between slopes and intercepts of Eqn. (3.12) and the cutting coefficients are obtained from Eqn. (3.11) as,

$$\begin{Bmatrix} m_x \\ m_y \\ b_x \\ b_y \end{Bmatrix} = \begin{bmatrix} \frac{a}{2\pi} & -\frac{a}{4} & 0. & 0. \\ \frac{a}{4} & \frac{a}{2\pi} & 0. & 0. \\ 0. & 0. & \frac{a}{\pi} & -\frac{a}{\pi} \\ 0. & 0. & \frac{a}{\pi} & \frac{a}{\pi} \end{bmatrix} \begin{Bmatrix} K_{tc} \\ K_{rc} \\ K_{te} \\ K_{re} \end{Bmatrix}. \tag{3.13}$$

Inserting the slopes and intercepts of lines associated with average feed and normal forces shown in Figure 3-7 into Eqn. (3.13) one obtains the cutting force constants of the Aluminum block in half immersion milling. These cutting force coefficients are reported in Table 2.

**Table 2: Identified average cutting force coefficients for a half-immersion down milling cutting experiment**

| ***Shear force coefficients [N/mm$^2$]*** | | ***Edge force coefficients [N/mm]*** | |
|---|---|---|---|
| $\boldsymbol{K_{tc}}$ | *1033.1* | $\boldsymbol{K_{te}}$ | *15.6* |
| $\boldsymbol{K_{rc}}$ | *330.0* | $\boldsymbol{K_{re}}$ | *20.3* |

The identified force coefficients indicate shear forces are much higher than the edge forces in the milling operations which is consistent with the physics involved in the machining. The next section verifies the validity of obtained cutting coefficients in more details.

### 3.2.3. Cutting Force Simulation using Average Cutting Force Coefficients

The identified cutting force coefficients were employed in the mechanistic milling model of Section 3.1 to predict the instantaneous cutting forces in both feed and normal directions.

Figure 3-8 and Figure 3-9 compares the model predictions versus experimental results for the four measured feed rates. As can be seen from this comparison the mechanistic model well represents the actual cutting forces. The deviations between analytical model predictions and observed behavior are mainly due to harmonic forces created by the spindle vibrations.

Another effect which contributes to the deviation of simulation results from observed behavior in milling operation is tool nose radius. The nose radius contribution is neglected in the mechanistic model.

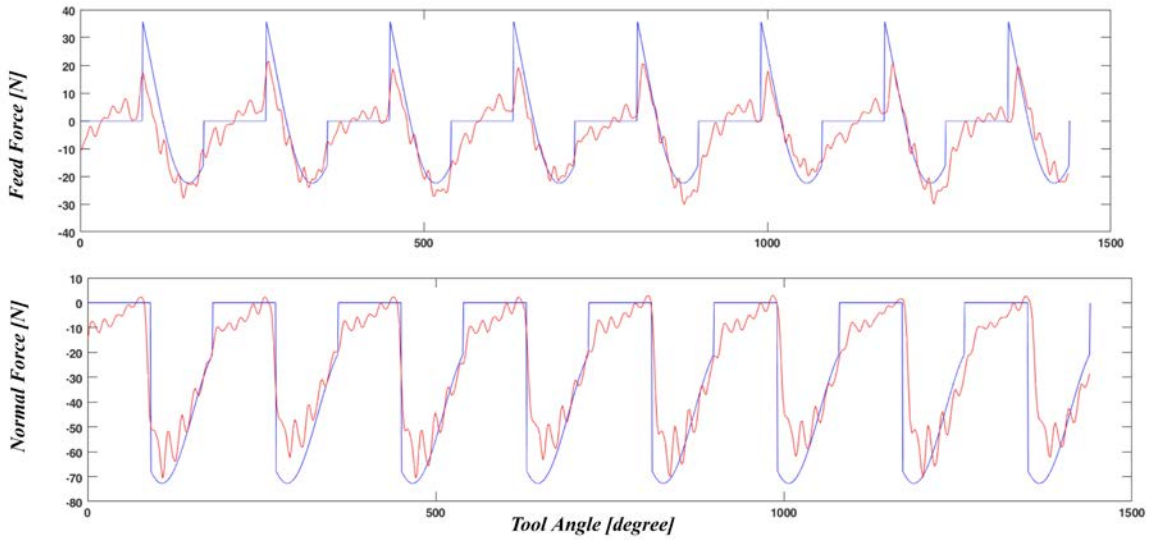


*a) 400 mm/min Feedrate*

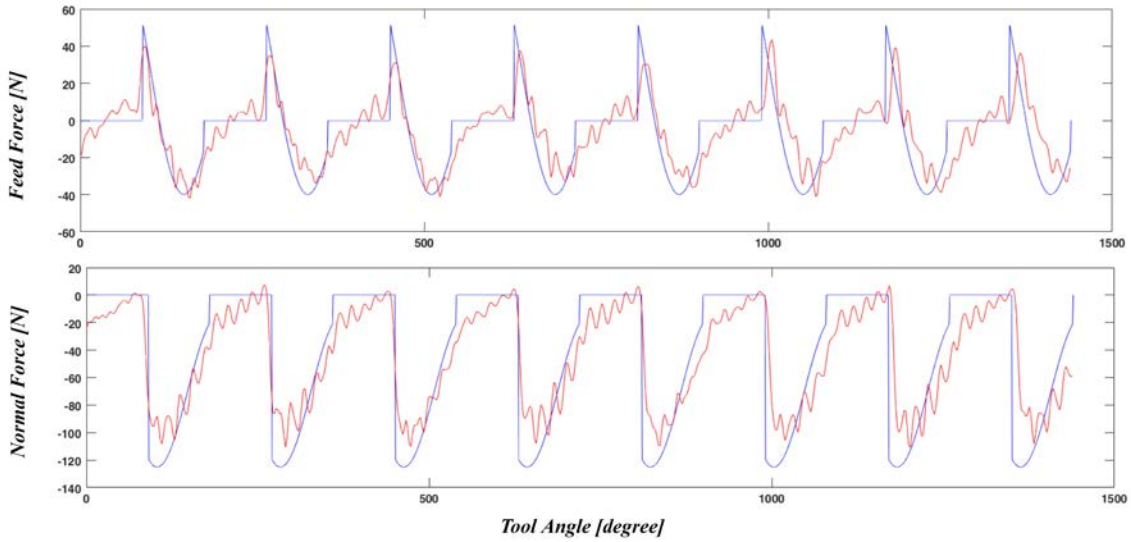


*b) 800 mm/min Feedrate*

**Figure 3-8: Comparison between simulated and measured forces for AL-6061 machining (1)**

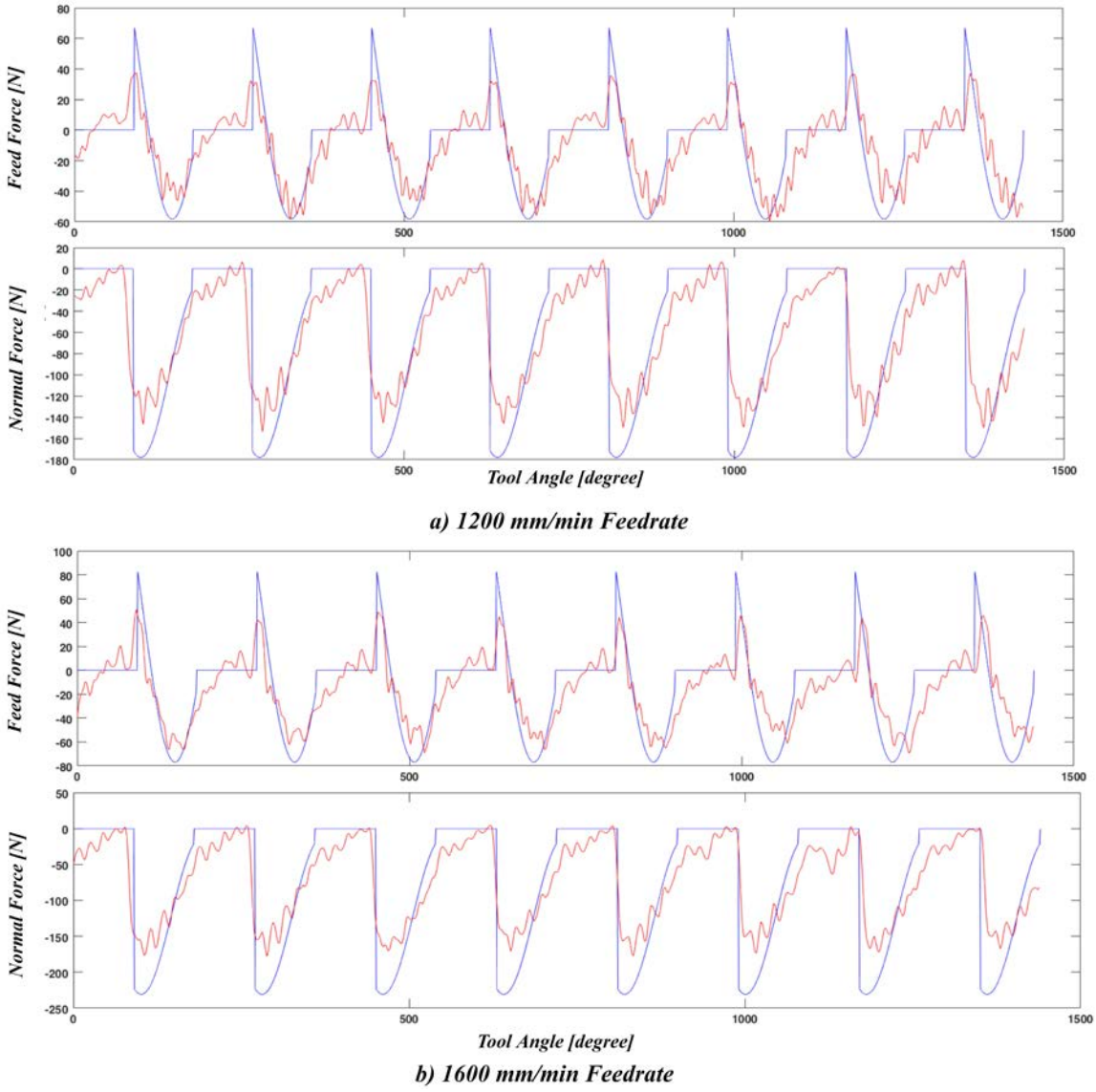


**Figure 3-9: Comparison between simulated and measured forces for AL-6061 machining (2)**

The mechanistic milling force model presented in this chapter along with the employed experimental test setup will be used in the following chapters to identify CFRP cutting constants in millings.

# Chapter 4
# Mechanistic Cutting Force Modeling for Milling CFRP

During the manufacturing process of CFRP components, it is usually necessary to carry out a post-machining step in order to meet the required geometric tolerances. Milling is one of the popular methods performed in order to accomplish this task. To fully understand the behavior of the material under the influence of various cutting parameters and to optimize the whole machining process, one needs to study a model which predicts the cutting forces. These models vary due to anisotropic CFRP's material properties when applying for Unidirectional (UD) and multi-directional (MD) composites. Also, the anisotropic nature of CFRP's causes a different chip formation mechanics from ductile metals. This imposes high wear in the tool and significantly changes the cutting forces during machining.

Due to the significant difference between material properties and characteristics of composites and metals, the fundamentals of metal cutting are not directly applicable to composites. In metal machining, the chip is formed through the plastic deformation of the material; as the cutting tool advances, a continuous chip is formed through shearing and plastic deformation of the material. In composites, however, the anisotropic and nonhomogeneous nature of the material makes the machining process highly dependent on the fiber orientation.

## 4.1. CFRP Laminates Milling Processes

Composite laminates are made by stacking up plies which may possess different fiber orientations. Fiber orientation angle, $\theta$, is defined as the angle measured counterclockwise between the cutting tool feed direction and the fiber orientation as shown in Figure 4-1. For unidirectional layers, $\theta$ is constant for all of the fibers, but in multi-directional layers, theta varies from one fiber to another.

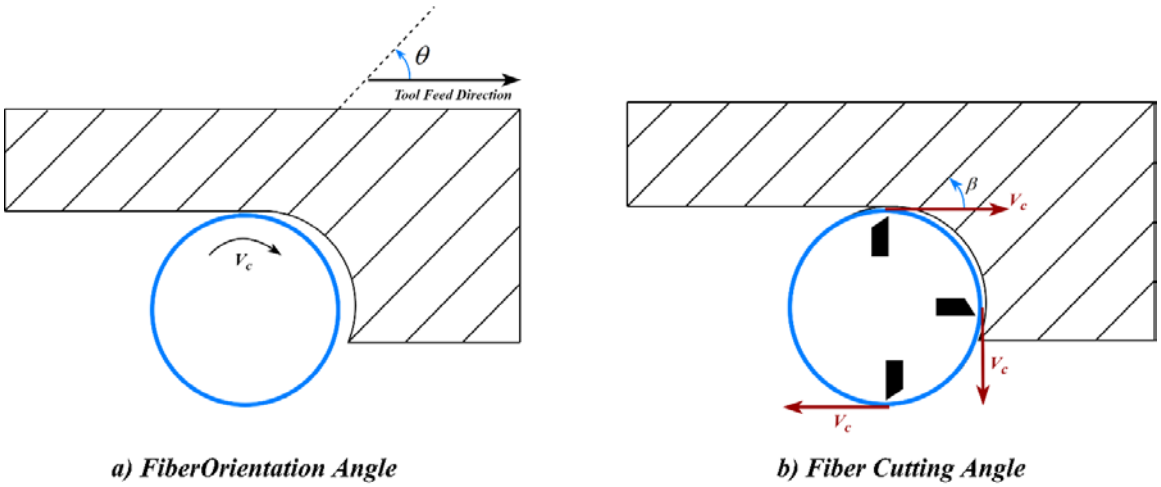


**Figure 4-1: Difference between fiber orientation angle and fiber cutting angle**

Fiber cutting angle, $\beta$, is the angle between the fiber that is being cut and cutting speed direction, i.e. the tangential direction of the tool at the fiber intersection (Figure 4-1). The fiber cutting angle changes continuously during the engagement of the cutting edge. The reason for this is the rotary cutting motion of the tool. Figure 4-2 illustrates the change in the fiber cutting angle for three different fiber orientations during slot milling.

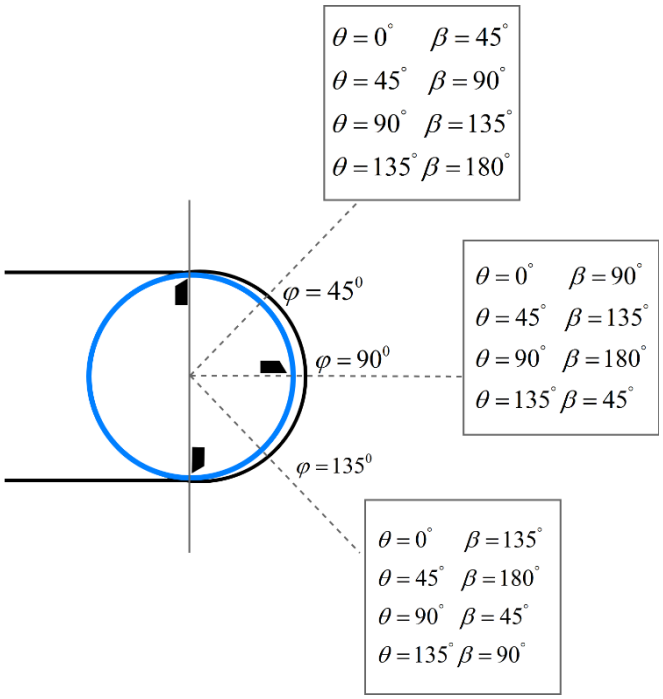


**Figure 4-2: Fiber cutting angles at different fiber orientation** [27]

In UD layers, the instantaneous fiber cutting angle is expressed in terms of immersion angle, $\varphi$, and fiber orientation angle, $\theta$ as [27]

$$\beta_{\varphi,\theta} = \varphi + \theta \text{ if } \beta \geq \pi \text{ then } \beta = \text{mod}(\beta, \pi) \tag{4.1}$$

With a varying fiber cutting angle, different chip formation mechanisms occur, such as bending, buckling, compression or shear. Four groups with similar chip formation mechanisms are identified, dividing the fiber cutting angle from $0^o \leq \beta \leq 180^o$ into four specific intervals as shown in Figure 4-3. These intervals are defined as [1]:

i. $\beta = 0^o / 180^o$: For a fiber cutting angle of $0^o$ and a positive rake angle tool, the cutting tool applies pressure in the direction of the cut as it advances in the work material. This creates compression in fiber direction resulting buckling, peeling of the matrix and inter-laminar crack.

ii. $15^o < \beta < 75^o$: At this range of fiber cutting angle and positive rake angle cutting tool, the tool edge radius becomes a significant factor. If the tool edge radius is comparable to the fiber diameter, compressive stresses at the contact point of the tool and the fibers result in crushing of the fibers. Following the crushing, the fiber matrix interface experiences a shear failure along the interface as it moves away from the cutting zone. Cracks are generated both above and below the cutting plane.

iii. $\beta = 90^o$: At this fiber cutting angle, chips fracture along the fiber-matrix interface due to high inter-laminar shear stresses. Both matrix and fibers experience shear force and compression.

iv. $105^o < \beta < 165^o$: In these fiber cutting angles, the dominant mechanism is fracturing of fibers due to bending and inter-laminar failure. As a result, fibers are peeled from the surface. An elastic recovery takes place and fibers sticking out from the surface contact the flank face of the tool.

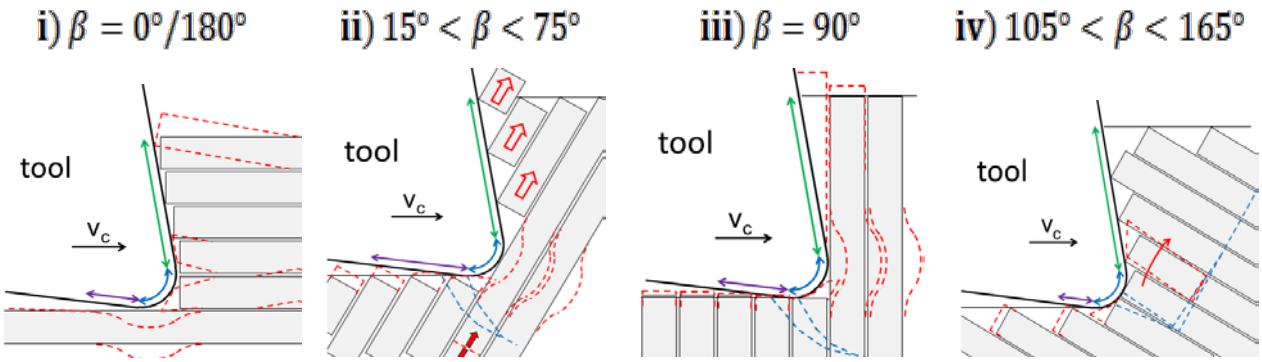


**Figure 4-3: Chip formations at different fiber orientations** [1]

Each of these intervals has an angular gap of 15° to the adjacent interval. The cutting mechanisms of the adjacent intervals mix in these angular gap regions.

## 4.2. Geometrical Modeling of CFRP Milling

Analyzing cutting conditions and cutting forces applied during CFRP machining requires precise knowledge of tool/fiber/matrix geometrical parameters such tool immersion angle, $\varphi$, fiber orientation angle, $\theta$, fiber cutting angle, $\beta$, along the machining tool path. These parameters are usually changed continuously especially during machining of a complex toolpath.

The kinematics of tool and workpiece are required during machining as input parameters to the mechanistic force models. There are several techniques employed in modeling this kinematics including dexel-models which are commonly used due to their superior computational capabilities. One of the simplest dexel models is two-dimensional arrays of lines or dexels. Each dexel can store data along its line's length, and can thus represent a volume with very high accuracy in one direction compared to the grid layer. The Tri-dexel model (volumetric pixel), as shown in Figure 4-4, is a three-dimensional grid of cells, where each cell can store data such as density or the time step when the element is cut.

In CFRP milling, Ref. [32] modelled carbon fibers as dexels, which are geometrically cut by a milling tool represented as a circle. Similar approach is used in this thesis to

compute the geometry of fiber cutting. Using a dexel model the tool immersion angle, $\varphi$, fiber orientation angle, $\theta$, fiber cutting angle, $\beta$, at each instant or time step $t(i)$ along the machining toolpath is determined. Also one may obtain the number and lengths of fibers cut per revolution of the tool using the geometrically defined dexel model.

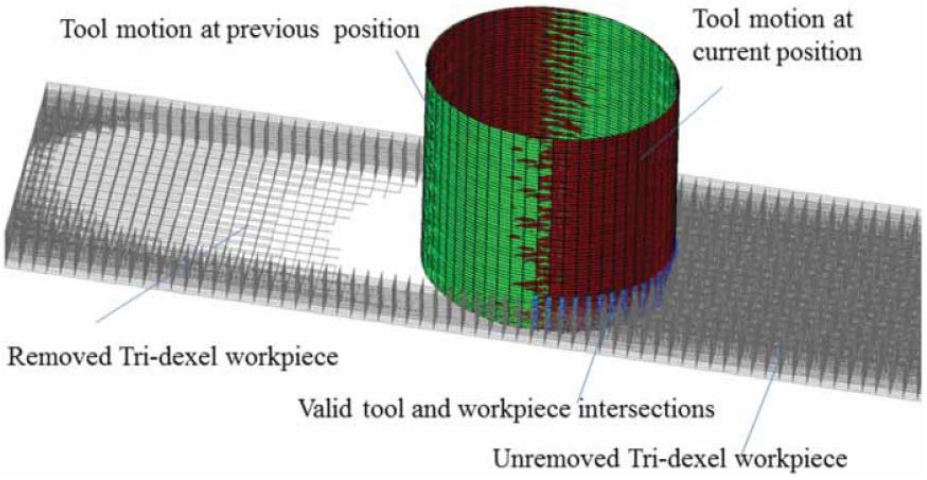


**Figure 4-4: Tri-dexel representation of a tool and workpiece** [33]

The machined chip is represented with points cloud corresponding to the outer surface of the removed chip geometry. The chip geometry is defined using the angular discretisized chip thickness $h(\varphi, z)$ with the start- and exit angles $\varphi_{st}$ , $\varphi_{ex}$. As the chip geometry varies along the cutting edge the chip is discretized into discs of the height $dz$ and in angular direction in $d\varphi$ as shown in Figure 4-5.

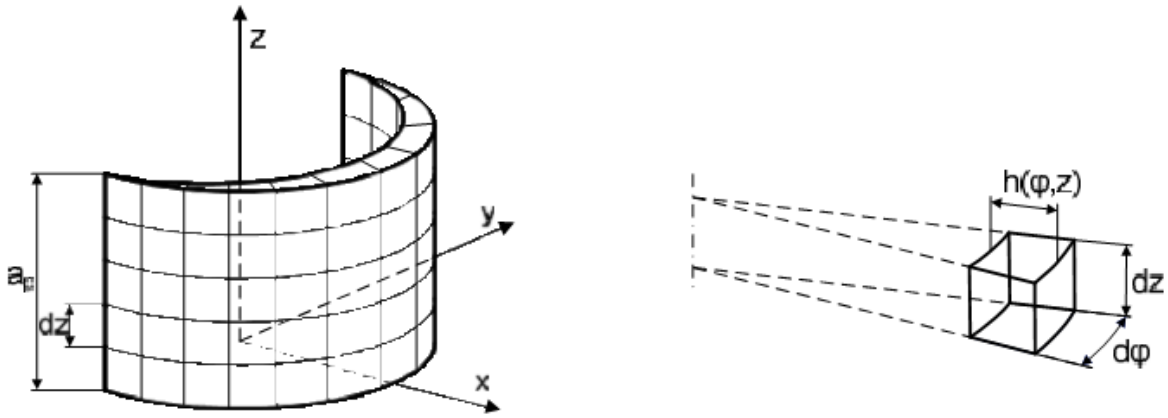


**Figure 4-5: Discretisiced chip geometry** [34]

The chip thickness is determined in three steps as defined in [34]:

- Initially, the point cloud is subdivided into disks of the height $dz$.
- Next inside of each disc the maximum angular points is defined as restricting points by $\varphi_{st}$, *and* $\varphi_{ex}$ (Figure 4-6 a). Due to the complex contact conditions and hence the complex chip geometries, the start and exit angles may vary over the depth of cut $a_p$.
- The analytic chip geometry of each disk can be calculated based on the cylindrical form of the cutter at the discrete time of $t(i)$ and $t(i-1)$.

The area between the start angle $\varphi_{st}$ and exit angle $\varphi_{ex}$ is discretized into multiple subareas with the angular distance $d\varphi$. The value of the discrete chip thickness $h(\varphi, z)$ in respect of $\varphi$ can be calculated by a line intersection with the two cylinders in the final step (Figure 4-6 b).

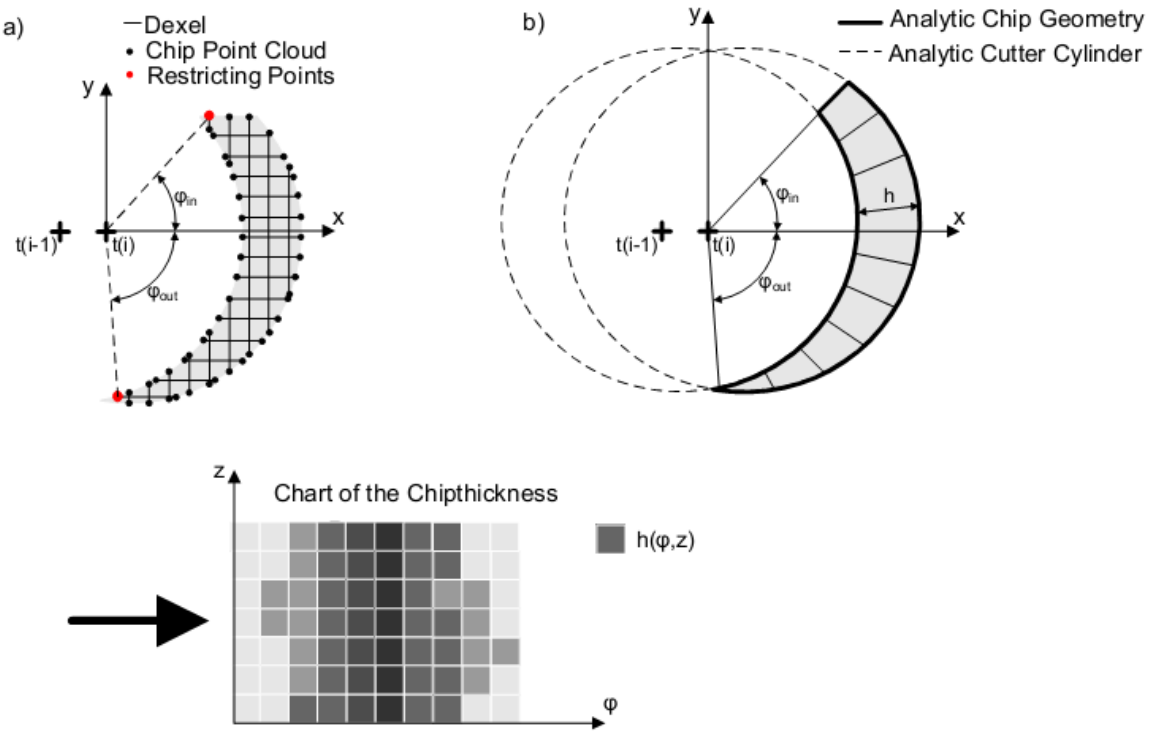


**Figure 4-6: Calculation of the chip thickness $h(\varphi, z)$** [34]

In UD-CFRP machining with a small depth of cut, one may employ a 2D dexel model and the discrete chip thickness as a function of tool immersion angle, i.e. $h(\varphi)$. The experiments conducted in this thesis are milling operations of UD-CFRPs and a MATLAB program is developed to calculate parameters such as instantaneous fiber length and its cutting angle. The inputs of the program consist of the fiber orientation, 2D tool-path geometry, endmill diameter, and the flutes start- and exit angles $\varphi_{st}$, $\varphi_{ex}$. The output of the MATLAB program is the instantaneous fiber cutting angle and fiber length at each flute of the tool.

Figure 4-7 to Figure 4-9 represent the program outputs for a UD-CFRP half-immersion up-milling with the fiber orientation of 30$^{o}$. The program considers the tool as a circle with radius *R*, which shifts along 2D tool path geometry with the amount of chip load, *c*. Intersections of the two circles shifted along the tool path with a line representing the fiber provides the fiber length, as shown in Figure 4-7 and Figure 4-8. Figure 4-9 shows the instantaneous fiber cutting angle of flute and is calculated using the tangential slope of the circle and the slope fiber at the intersection point.

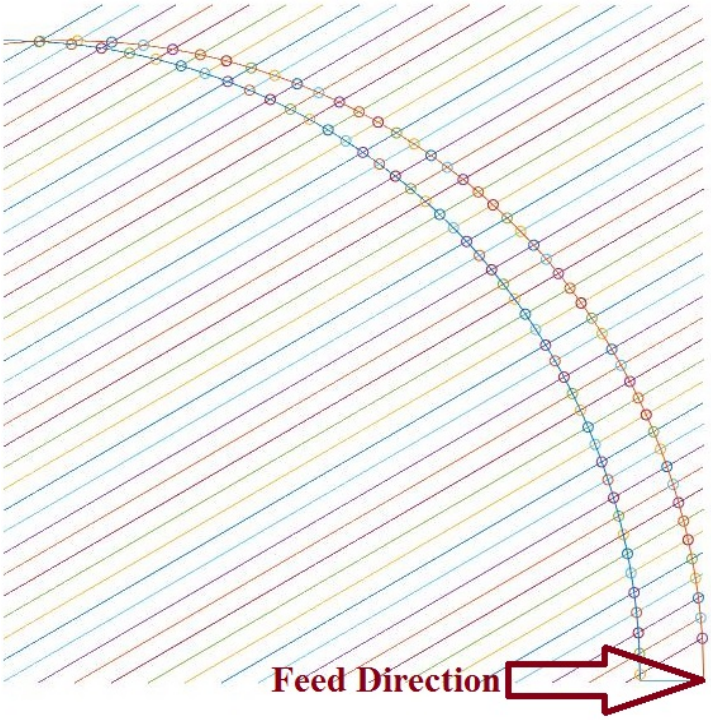


**Figure 4-7: Geometrical representation of UD-CFRP half immersion up milling in MATLAB program**

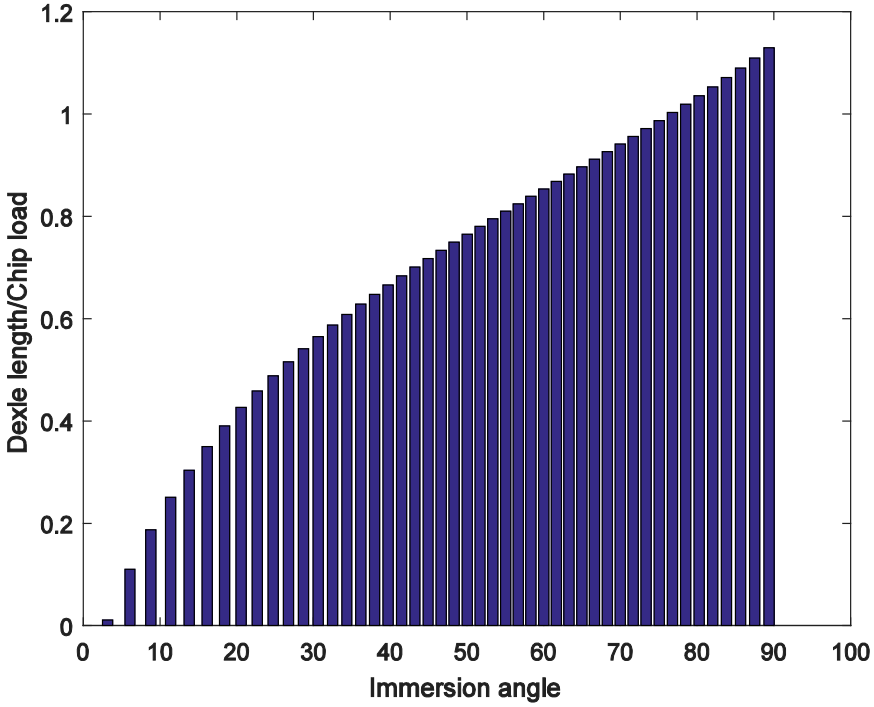


**Figure 4-8: Non-dimensional Dexle length**

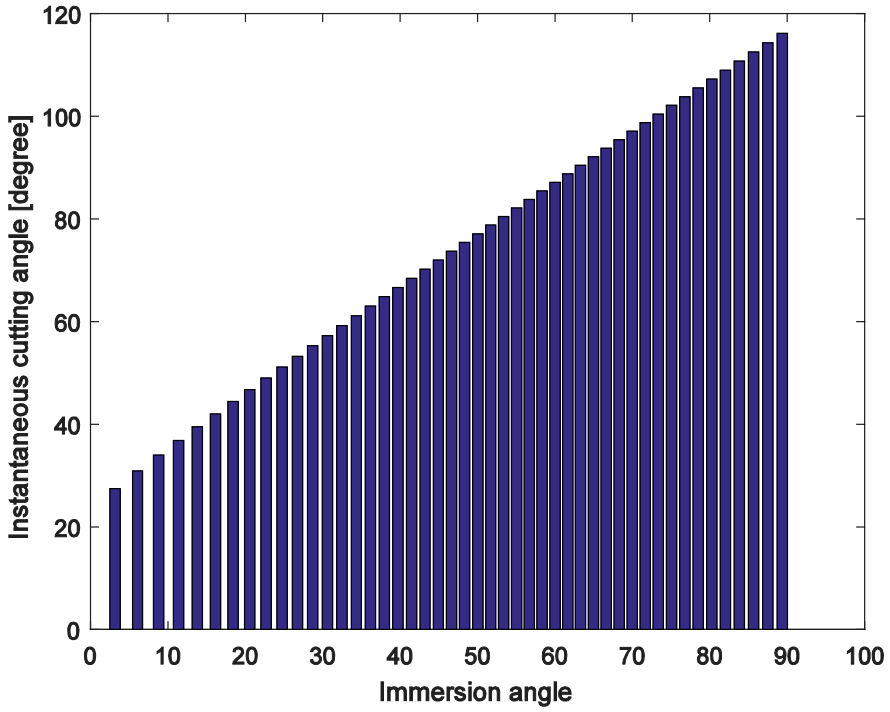


**Figure 4-9: Instantaneous fiber cutting angle of flute**

The output of the MATLAB program for different parameters is customized based on the needs for the case under study. As an example, the fiber orientation angle, $\theta$, and the instantaneous fiber cutting angle, $\beta$, of a 2D semi-circular tool path in up milling with 50% radial immersion, that is studied in chapter 5, is calculated and represented in Figure 4-10 and Figure 4-11 respectively. Figure 4-10 shows the fiber orientation angle continuously increasing from $90^o$ to $270^o$ when the tool moves along the toolpath. In Figure 4-10 the toolpath is normalized to its length and it is varied from zero to unity.

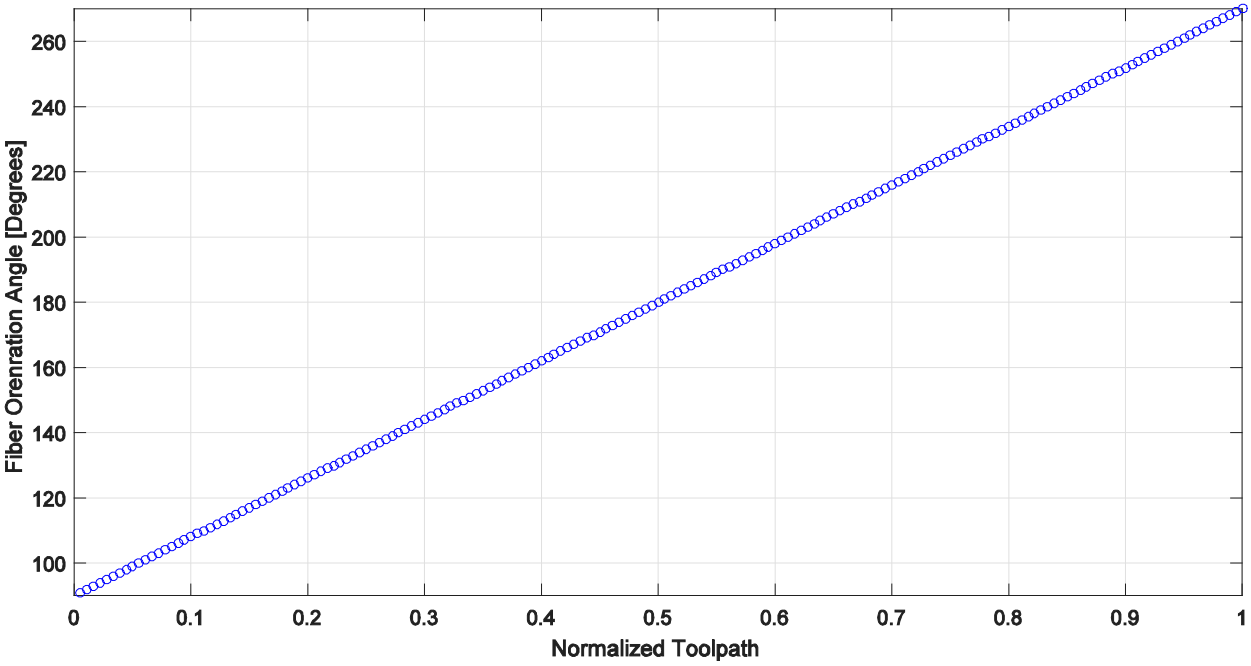


**Figure 4-10: Fiber orientation angle, $\theta$, in a semi-circular tool path**

Figure 4-11 shows the instantaneous fiber cutting angle $\beta$ of each flute of the two fluted tool at three fiber orientation angles of 90º, 150º, and 210º. In Figure 4-11 the tool immersion angle $\phi$ is varied between 0º to 360º and as each flute engages, the fiber cutting angle is shown. When the first flute is engaged in fiber orientation angle of $\theta = 90^o$ the tool cutting angle is $\phi = 0^o$ and the cutting angle $\beta = \text{mod}(\theta + \phi, 180^o)$ is equal 90º and it increases up to 180º as $\phi$ becomes $90^o$. Next at $\theta = 150^o$ the first flute engagement range is $0^o \le \phi \le 90^o$ which results $150^o \le \beta \le 180^o$ and $0^o \le \beta \le 60^o$. Similarly, when $\theta = 210^o$, the first flute engagement range is again $0^o \le \phi \le 90^o$ which results $30^o \le \beta \le 120^o$. The second flute follows the same cutting angles as the first flute due to the fact that changes in fiber orientation angle $\theta$ in each tool revolution is negligible.

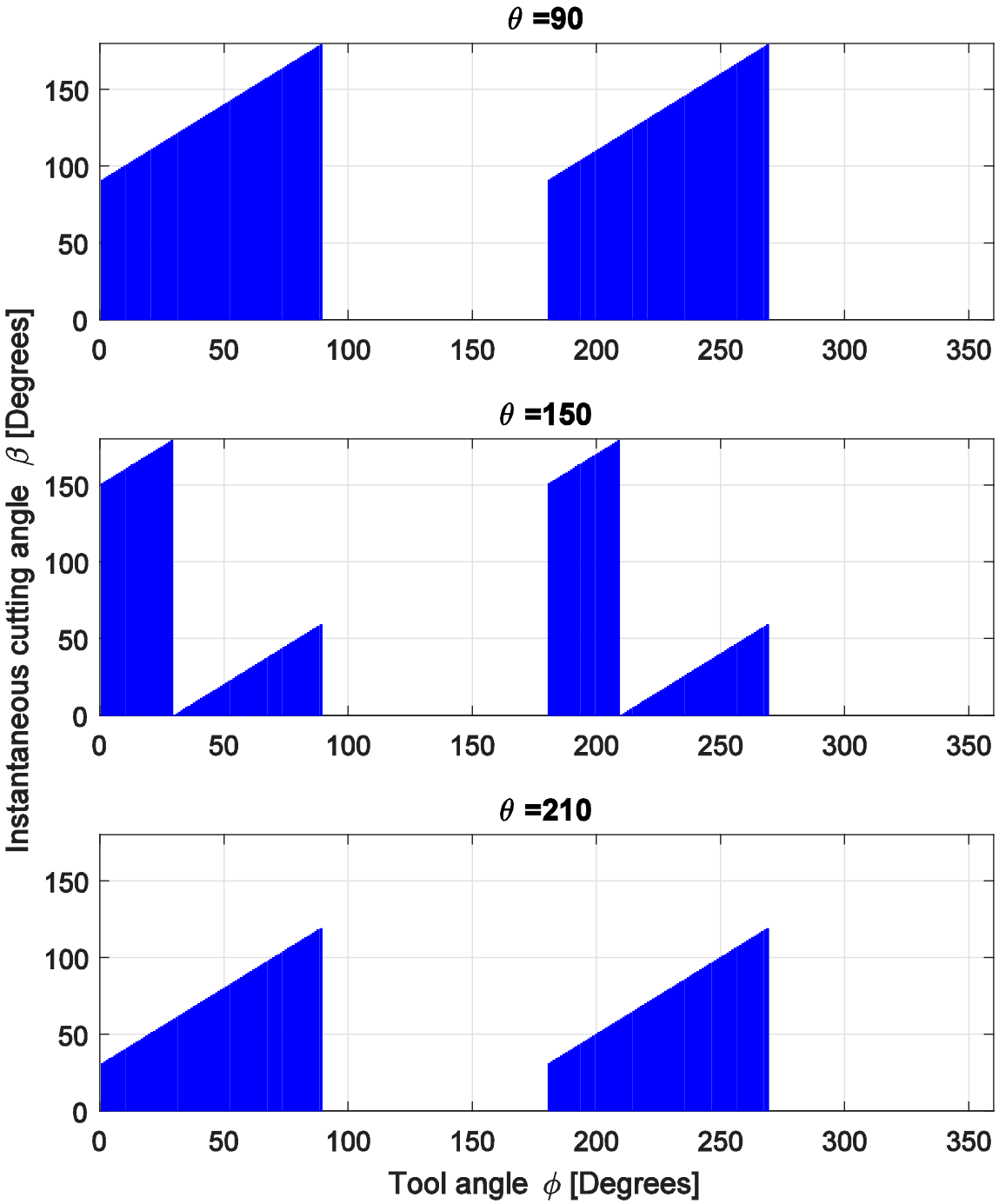


**Figure 4-11: instantaneous fiber cutting angle, $\beta$, in a semi-circular tool path**

### 4.3. Mechanistic Force Model for Milling CFRP

Figure 4-12 presents cutting forces acting on the tooltip during UD-CFRP milling operation where $F_t$ is the tangential force, $F_r$ represents the radial force directed toward the center and $c$ is the feed rate.

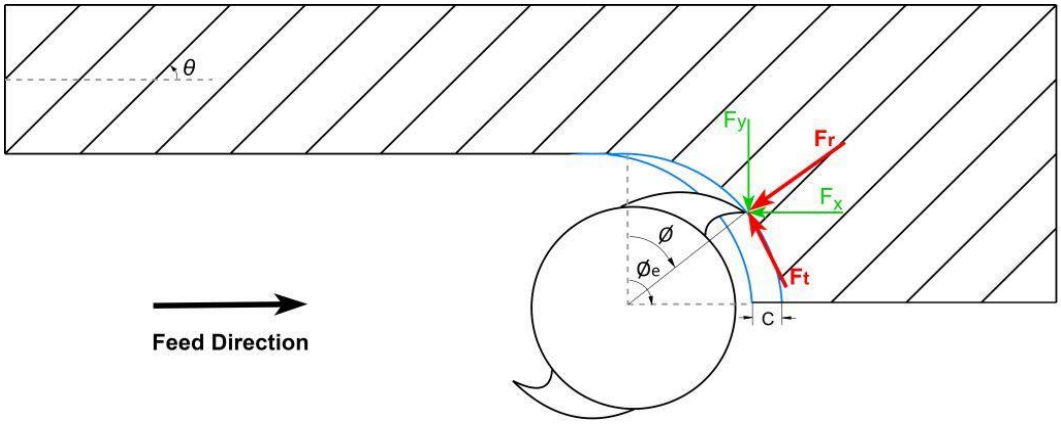


**Figure 4-12: Cutting forces acting on tooltip during CFRP milling**

The linear mechanistic cutting force model, used in Chapter 3, was modified by [27] to include the effect of different cutting mechanics in various fiber cutting angles in CFRP milling. In their model, cutting force coefficients were assumed to be functions of the fiber cutting angle, resulting in the following mechanistic model of radial and tangential forces:

$$f_{jt}(\varphi,\beta) = K_{tc}(\beta)ah(\varphi) + K_{te}(\beta)a, \tag{4.2}$$

$$f_{jr}(\varphi,\beta) = K_{rc}(\beta)ah(\varphi) + K_{re}(\beta)a, \tag{4.3}$$

where $a$ is the axial depth of cut, $K_{tc}(\beta)$ and $K_{rc}(\beta)$ are the cutting force functions, $K_{te}(\beta)$ and $K_{re}(\beta)$ are edge force functions. These functions are defined using fiber cutting angle as follows.

As described in the previous section, the mechanics of the chip generated during milling of CFRP strongly depends on the fiber cutting angle, which changes at different immersion angles. To account for the variation of chip formation mechanics at various

fiber cutting angles, the cutting and edge force coefficients are assumed to be functions of the fiber cutting angle. The variation of the fiber cutting angle is within the range of $0 \le \beta \le \pi$ which is half of the tool revolution period, $0 \le \varphi \le 2\pi$. Therefore [35] modeled the cutting force coefficients as periodic functions represented by their corresponding finite Fourier series:

$$K_{mn}(\beta) = \sum_{i=0}^{M} K_{mn,ic} \cos(2i\beta) + K_{mn,is} \sin(2i\beta), m = t, r, n = c, e \tag{4.4}$$

One notices the expansion is in terms of $2\beta$ to respect the fact that fiber cutting angle ranges from zero to $\pi$. The forces acting on the tool can be expressed as the sum of all radial and tangential forces acting on the tool with $N$ flutes projected to the feed and normal directions (shown as *x* and *y* respectively in Figure 4-12) as

$$\begin{Bmatrix} F_x(\theta) \\ F_y(\theta) \end{Bmatrix} = \sum_{j=1}^{N} g(\varphi_j) \begin{bmatrix} -\cos(\varphi_j) & -\sin(\varphi_j) \\ \sin(\varphi_j) & -\cos(\varphi_j) \end{bmatrix} \begin{Bmatrix} f_t(\varphi_j, \beta) \\ f_r(\varphi_j, \beta) \end{Bmatrix} \tag{4.5}$$

where $g(\phi_j)$ is an indicator function, which specifies whether the cutting edge is in contact with the work-piece or not. This function is unit when there is a contact, i.e. $\phi_s \le \phi_j \le \phi_e$, and zero elsewhere.

$$g(\varphi_j) = Heaviside(\varphi_s - \varphi_j) - Heaviside(\varphi_e - \varphi_j) \tag{4.6}$$

The cutting forces acting on a CFRP workpiece are determined using the mechanistic model discussed in this chapter. An important prerequisite of cutting force determination is to define the cutting force functions of Eqn. (4.4). [35] presented an experimental approach to identify the periodic cutting force coefficients in Eq. 4.4 based on the average of the measured cutting forces in various feedrates and fiber orientations. The same approach is used in this thesis, which is explained in section 4.4.

## 4.4. Cutting Force Coefficients Identification for UD-CFRP Milling

In the current study, we are interested in identifying the Fourier series coefficients in Eq. (4.4). The concept is the same as the procedure followed in the previous chapter for identifying average cutting force coefficients in metal cutting with some differences in details.

The average cutting force per tooth passing period for UD-CFRP can be determined by integrating Eq. (4.5) over one tool revolution and dividing by pitch angle

$$\overline{F}(\theta)=\begin{Bmatrix} mean(F_x(\theta)) \\ mean(F_y(\theta)) \end{Bmatrix}=\frac{1}{\varphi_p}\sum_{j=1}^{N}\int_{\varphi_{st}}^{\varphi_{ex}} g(\varphi_j)\begin{bmatrix} -\cos(\varphi_j) & -\sin(\varphi_j) \\ \sin(\varphi_j) & -\cos(\varphi_j) \end{bmatrix}\begin{Bmatrix} f_t(\varphi_j,\beta) \\ f_r(\varphi_j,\beta) \end{Bmatrix} d\varphi \qquad (4.7)$$

By substituting $f_{jt}$ and $f_{jr}$ from Eq. (4.2) and Eq. (4.3) into Eq. (4.7), the average cutting forces can be expressed by a linear function of feed rate, $c$, and an offset contributed by the edge forces which is defined as

$$\begin{aligned} mean(F_x(\theta)) &= b_{0x}(\theta)+b_{1x}(\theta)\times c \\ mean(F_y(\theta)) &= b_{0y}(\theta)+b_{1y}(\theta)\times c \end{aligned} \qquad (4.8)$$

where $b_{0x}(\theta), b_{1x}(\theta), b_{0y}(\theta)$, and $b_{1y}(\theta)$ are linear functions of the Fourier coefficients in Eq. (4.4). In the case wherein Eq. (4.4), $M$ is set to unity this relation can be expressed as

$$\begin{Bmatrix} b_{0x}(\theta) \\ b_{1x}(\theta) \\ b_{0y}(\theta) \\ b_{1y}(\theta) \end{Bmatrix} = \begin{bmatrix} B_{1,1} & B_{1,2} & \cdots & & B_{1,12} \\ B_{2,1} & \ddots & & & \vdots \\ \vdots & & & \ddots & \vdots \\ B_{4,1} & & \cdots & & B_{4,12} \end{bmatrix} \begin{Bmatrix} K_{tc,0c} \\ K_{tc,1c} \\ K_{tc,1s} \\ K_{te,0c} \\ K_{te,1c} \\ K_{te,1s} \\ K_{rc,0c} \\ K_{rc,1c} \\ K_{rc,1s} \\ K_{re,0c} \\ K_{re,1c} \\ K_{re,1s} \end{Bmatrix} \tag{4.9}$$

Entries of $B_{i,j}, i = 1 \cdots 4, j = 1 \cdots 12$ are functions of $\theta$. The entries of matrix **B** given in Eqn. (4.9) are provided in the following, assuming an up-milling half-immersion operation with the tool entry and exit angles of $\varphi_{st} = 0$, $\varphi_{ex} = \pi$ with a two fluted tool, i.e. *N=2*. All entries are normalized by the edge contact length $a$.

$$B_{1,1} = \frac{1}{2\pi}$$
$$B_{1,2} = \frac{1}{8} - \frac{cos^2(\theta)}{4}$$
$$B_{1,3} = \frac{sin(\theta)cos(\theta)}{4}$$
$$B_{1,4} = 0$$
$$B_{1,5} = 0$$
$$B_{1,6} = 0$$
$$B_{1,7} = -\frac{1}{4}$$
$$B_{1,8} = \frac{sin(\theta)cos(\theta)}{4} + \frac{cos^2(\theta)}{\pi} - \frac{1}{2\pi}$$
$$B_{1,9} = \frac{cos^2(\theta)}{4} - \frac{sin(\theta)cos(\theta)}{\pi} - \frac{1}{8}$$
$$B_{1,10} = 0$$
$$B_{1,11} = 0$$
$$B_{1,12} = 0$$

$$B_{2,1} = 0$$
$$B_{2,2} = 0$$
$$B_{2,3} = 0$$
$$B_{2,4} = \frac{1}{\pi}$$
$$B_{2,5} = \frac{2sin(\theta)cos(\theta) - 4cos^2(\theta) + 2}{3\pi}$$
$$B_{2,6} = \frac{4sin(\theta)cos(\theta) + 2cos^2(\theta) - 1}{3\pi}$$
$$B_{2,7} = 0$$
$$B_{2,8} = 0$$
$$B_{2,9} = 0$$
$$B_{2,10} = -\frac{1}{\pi}$$
$$B_{2,11} = \frac{2sin(\theta)cos(\theta) + 4cos^2(\theta) - 2}{3\pi}$$
$$B_{2,12} = \frac{2cos^2(\theta) - 4sin(\theta)cos(\theta) - 1}{3\pi}$$

$$B_{3,1} = \frac{1}{4}$$
$$B_{3,2} = \frac{2 - \pi sin(\theta)cos(\theta) - 4cos^2(\theta)}{4\pi}$$
$$B_{3,3} = \frac{\pi + 8sin(\theta)cos(\theta) - 2\pi cos^2(\theta)}{8\pi}$$
$$B_{3,4} = 0$$
$$B_{3,5} = 0$$
$$B_{3,6} = 0$$
$$B_{3,7} = \frac{1}{2\pi}$$
$$B_{3,8} = \frac{1 - 2cos^2(\theta)}{4}$$
$$B_{3,9} = \frac{sin(\theta)cos(\theta)}{4}$$
$$B_{3,10} = 0$$
$$B_{3,11} = 0$$
$$B_{3,12} = 0$$

$$B_{4,1} = 0$$
$$B_{4,2} = 0$$
$$B_{4,3} = 0$$
$$B_{4,4} = \frac{1}{\pi}$$
$$B_{4,5} = \frac{2 - 2sin(\theta)cos(\theta) - 4cos^2(\theta)}{3\pi}$$
$$B_{4,6} = \frac{1 + 4sin(\theta)cos(\theta) - 2cos^2(\theta)}{3\pi}$$
$$B_{4,7} = 0$$
$$B_{4,8} = 0$$
$$B_{4,9} = 0$$
$$B_{4,10} = \frac{1}{\pi}$$
$$B_{4,11} = \frac{2sin(\theta)cos(\theta) - 4cos^2(\theta) + 2}{3\pi}$$
$$B_{4,12} = \frac{2cos^2(\theta) + 4sin(\theta)cos(\theta) - 1}{3\pi}$$

In order to identify the cutting force coefficients in Eq. (4.9), cutting experiments on UD-CFRP workpiece are conducted at a constant fiber orientation angle with a various set of federate and the average of the cutting forces in each test is computed which will give us an overdetermined set of equations from Eq. (4.8).

If the cutting experiment procedure is repeated for a number of different fiber orientation angles, an over-determined system is constructed by Eq. (4.9). This enables one to estimate the Fourier coefficients of cutting force functions. In the next chapter, this procedure is demonstrated in detail by using experimentally measured data.

## 4.5. Mechanistic Force Model for MD-CFRP Milling

In most practical cases MD-CFRP laminates are produced and their machining forces need to be determined. The MD-CFRP laminates consist of various numbers of layers for each direction. It may, for example, have a repeating $0^o/45^o/90^o/135^o$ fiber direction configuration. In order to adapt the milling force model to MD laminates, the tool is sectioned into a number of slices perpendicular to its rotation axis. Each slice thickness is considered equal to the thickness of the associated layer of the unidirectional laminate.

Fiber direction ($\theta$) is defined at each layer, and the fiber cutting angle ($\beta$) is calculated depending on the tool rotation angle ($\varphi$) at each layer in the milling force model. Cutting forces from each layer are superposed to calculate total milling forces [36].

# Chapter 5
# Experimental Procedure and Data Analysis

An experimental case study is presented in this chapter to identify the cutting constants of UD-CFRP workpiece in milling operations. This chapter reports the details of these experiments including the details of the test setup, test scenario, measured data analysis procedure, and the obtained cutting constants from measured experimental data. To demonstrate the success of the presented method in identifying cutting coefficients, predictions of cutting forces in a circular toolpath using the identified cutting coefficients are validated against experimental observations.

## 5.1. Experimental Procedure

A set of milling experiments are conducted to demonstrate the accuracy of the presented milling force modeling approach. These experiments are conducted using UD-CFRP. The following provides details of workpiece, tool, and milling operation conditions. Also, the measuring setup which includes dynamometer, data acquisition system, and the data logger system is described.

### 5.1.1. Composite Workpiece

The workpiece used in this study is a Unidirectional Carbon Fiber Reinforced Composite (UD-CFRP). It is a carbon epoxy laminate, cured in the autoclave. A pre-peg manufactured with unidirectional tape from Toray Inc., with a fiber volume content of 68% (by weight), was used to produce the laminate with a final thickness of approximately 30mm and cut to blocks of dimensions: 120*120*30mm. The following Table 3 gives a detailed description of the workpiece material.

**Table 3: Material properties of CFRP workpiece**

| Property | Fiber Fraction | Layup | Laminate Density | Tensile Strength | Tensile Modulus |
|---|---|---|---|---|---|
| **Value** | 68% | $[0]_{200}$ | 1.5 g/cm$^3$ | 5200 MPa | 250 GPa |

### 5.1.2. Cutting Tool

All experiments are carried out with a DIA-EDS end mill Manufactured by OSG Japan. The tool employed is a 2 fluted, 10mm diameter carbide end mill with a ~ 35° helix angle. The diamond coating has been chosen in order to minimize the tool wear during CFRP machining. Geometrical specifications of the tool are presented in Figure 5-1.

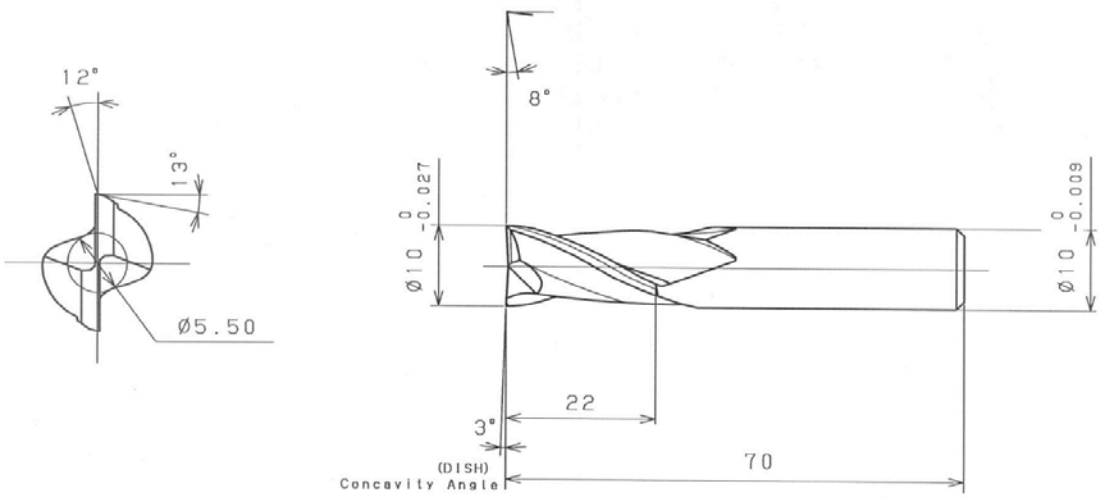


**Figure 5-1: DIA-EDS Ultra Fine Grain Diamond Coating** [37]

### 5.1.3. Experimental Setup

The setup used for conducting experiments and collecting cutting forces includes a CNC machine, a dynamometer, and a data acquisition system. The further detailed description is given in the following sections.

#### 5.1.3.1. The CNC Machine

The milling experiments were carried out on a 3-Axis vertical CNC machine capable of running up to a maximum spindle speed of 24000 rpm (Figure 5-2). This machine is equipped with a FANUC series 0i controller and a special dust collection system in order to gather all carbon fiber dust released during machining as it is hazardous and may cause lung damage in operators.

**Figure 5-2: 3-Axis vertical milling machine with a special dust collector**

### 5.1.3.2. The Dynamometer

A 9255C 3-component Kistler dynamometer is used for measuring cutting forces. The multicomponent dynamometer provides a dynamic and quasi-static measurement of the 3 orthogonal components of force acting from any direction onto the top plate. The dynamometer has high rigidity and consequently poses high natural frequency as indicated in Table 4. The high force measuring resolution enables very small dynamic changes to be measured in large forces. The dynamometer measures the active cutting force within the range given in Table 4 regardless of its application point [38].

**Table 4: Kistler 9255C Dynamometer Specification**

| Direction | Force Range [kN] | Natural frequency [kHz] |
|---|---|---|
| X | ±30 | 2.2 |
| Y | ±30 | 2.2 |
| Z | −10...+60 | 3.3 |

The force to be measured is introduced via a top plate and is distributed between four piezoelectric 3-component force sensors arranged between the base and top plates. Each of the sensors has three pairs of quartz plates, one sensitive to pressure in the tool axis, called z-direction, and the other two plates are sensitive to shear in the x and y directions respectively. The measurement is performed virtually without deformation of the dynamometer due to its high stiffness. In these four force sensors the force introduced is broken down into three components (Figure 5-3).


**Figure 5-3: Stationary 3 component dynamometer** [39]

### 5.1.3.3. Data Acquisition System

Cutpro software is used for storage and processing where the input is taken through an NI9234 four channel dynamic signal acquisition module. The measured signals from the dynamometer are conditioned and amplified using a multichannel charge amplifier Type 5070 from Kistler. There are multiple channels which can be set to take in different forces. The analog outputs are set to measure $F_x$, $F_y$, $F_z$ on Channels 1, 2, and 3 respectively. Amplified signals are digitized at 51.2KHz sampling rate by the data acquisition card. Figure 5-4 shows a schematic of how the data acquisition process works.

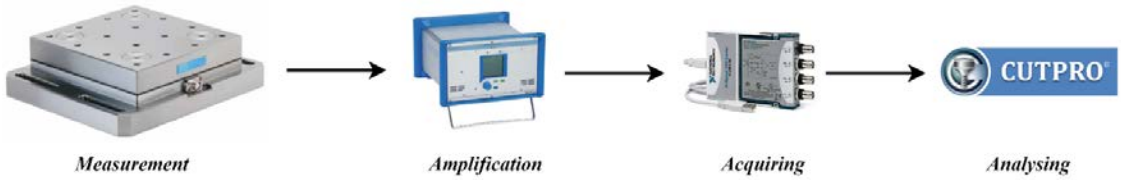


**Figure 5-4: Schematic of the data acquisition process**

### 5.1.4. Milling Process

The general procedure of the experiments performed for cutting CFRP workpiece is the same as the ones conducted for identifying cutting force coefficients for the metal workpiece in Chapter 3. The difference is that metals are isotropic material but CFRPs are anisotropic. This difference requires carrying out experiments at different fiber angle orientations. In the next section, the experiments carried out for identifying cutting force coefficients for a CFRP workpiece and the tool path used for verifying the model acquired are presented.

#### 5.1.4.1. Experiments for Identifying CFRP Cutting Constants

In order to identify the cutting force coefficients for a CFRP workpiece, it is needed to conduct milling experiments at different fiber orientation angles. The cutting forces are measured at least in 3 different fiber orientations as explained in Chapter 4 to be able to extract the cutting coefficients. In this study measurements of cutting forces on UD-CFRPs is performed in five different orientation angles as will be defined later in this chapter. Figure 5-5 shows the UD-CFRP workpiece clamped on the dynamometer. Sufficient torque is applied in order to make sure the workpiece is rigidly fixed to the dynamometer. This matter becomes more important because a diamond coated tool is used which has a good resistant to tool wear but sensitive in dealing with shocks.

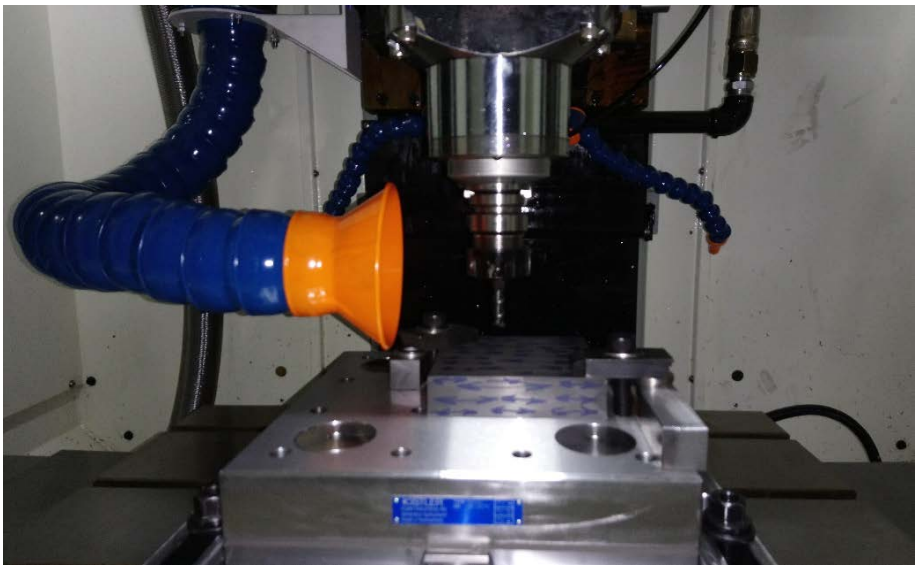

**Figure 5-5: Clamped CFRP workpiece on the dynamometer**

In this study, experiments were conducted at six different fiber orientation angles which includes $0^o / 30^o / 60^o / 90^o / 120^o / 150^o$ fiber orientation angles. Figure 5-6 presents a schematic of the milling process during these tests.

In each experimental test set, the axial depth of cut should be kept constant. In this research, cutting experiments were first performed at different depths of cut including 0.7mm, 1mm, and 2mm. It was found out that with 1mm axial depth of cut reasonable data can be captured and consequently a lot of workpiece waste was prevented. The spindle speed is also constant at all time. According to [40], the spindle speed is chosen to be 4000 rev/min, which is a proper speed for CFRP milling.

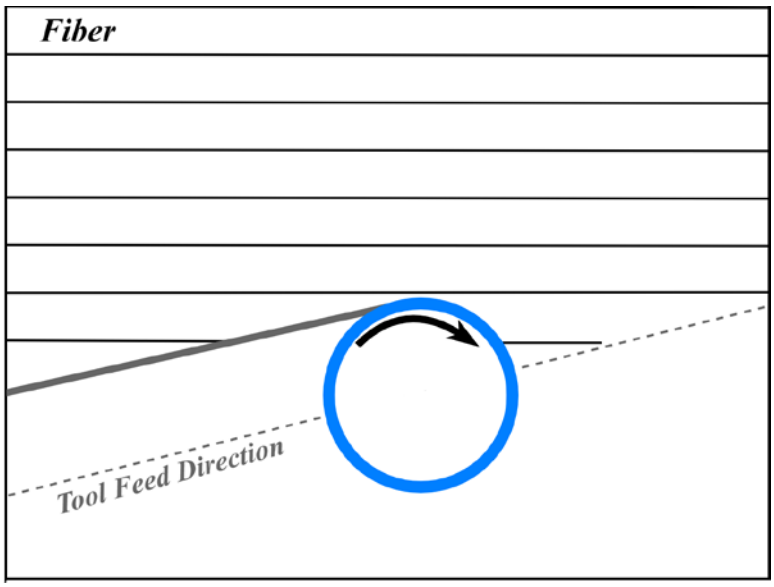


**Figure 5-6: Half immersion up milling for cutting force coefficient identification**

Half-immersion up-milling and down milling tests are conducted at different fiber orientations as specified previously; five different chip loads are chosen for the tests to be used at each fiber orientation, c = 0.05; 0.1; 0.15; 0.175; 0.2 mm/flute. Table 5 provides a summary of the milling experiments performed in order to identify the cutting force coefficients in CFRP.

**Table 5: Machining parameters used for CFRP cutting experiments**

| Machining Condition | Fiber Orientation Angle | Chip Load (mm/flute) | Spindle Speed (rpm) | Depth of cut (mm) |
|---|---|---|---|---|
| **Up/Down-Milling** | $0^o$ /$30^o$/$60^o$/$90^o$/$120^o$/$150^o$ | 0.05/0.1/0.15/0.175/0.2 | 4000 | 1 |

Following is a sample G-Code which was used for one of the cuttings experiments:

```
%
G17 G40 G49 G80
G90 G00 G54 X0. Y0.
G91 G28 Z0.
G90 G54 G00 X-10. Y-5.83
M6 T3
G43 H03 Z5.
M3 S4000
G01 F400 Z-2.
F400 X140. Y81.62
```

```
G91 G28 Z0.
M30
```

Figure 5-7 presents the data recorded from the cutting experiment conducted at a fiber orientation angle of 150 degrees at three of the defined chip loads.

During the experiments it was observed that the surface finish quality is affected by fiber orientations and the machining condition (up-milling or down milling), As for a fiber orientation angle of $120^{o,}$ the surface finish is in good shape in up milling but in down milling the result is different as shown in Figure 5-8. The low-quality surface finish is because of the wisps emerging from the work surface which occurs during machining and also affects the cutting data recorded and reduces its surface quality.

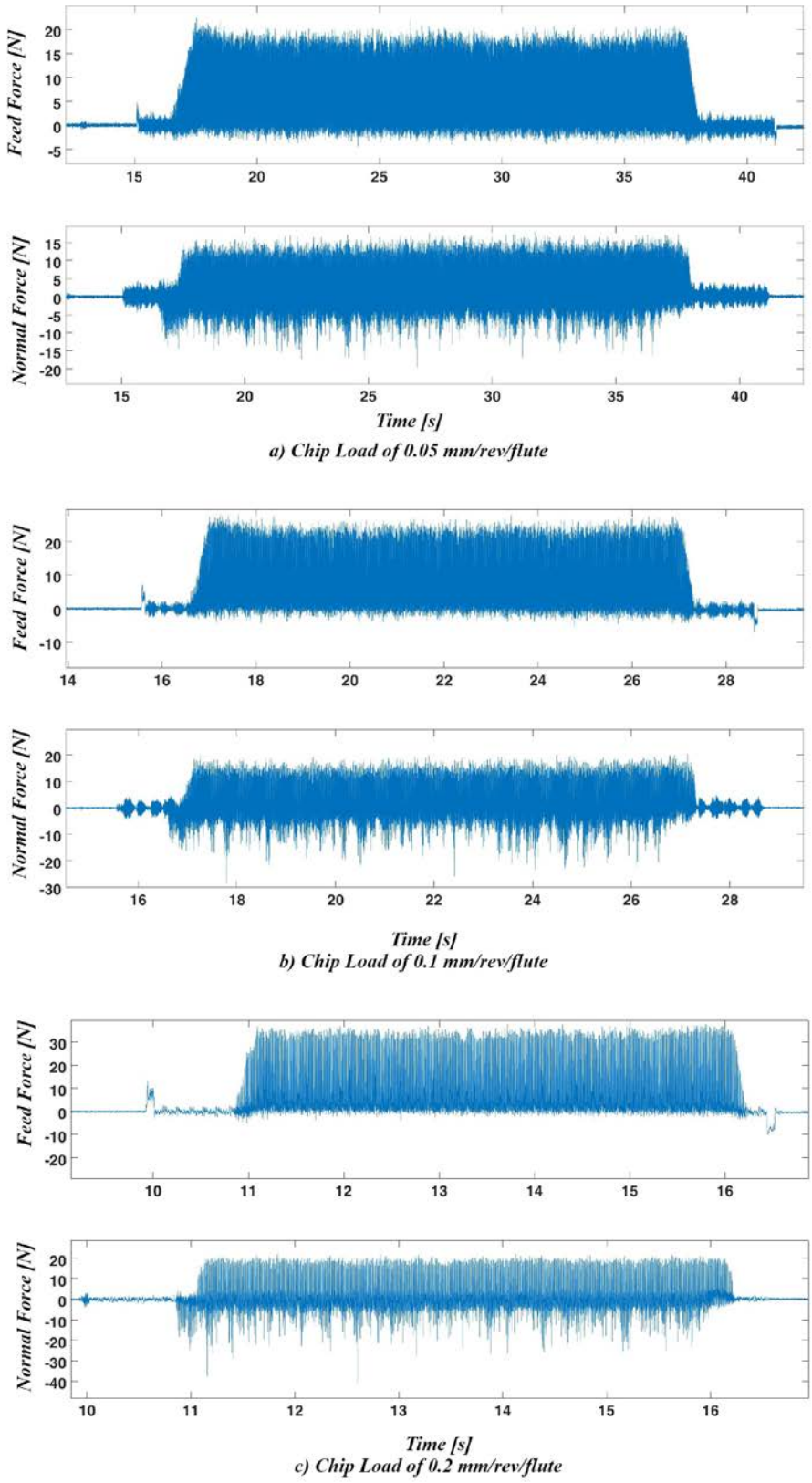


**Figure 5-7: Data Recorded from CFRP cutting with a fiber orientation angle of 150º**


a) Half immersion up-milling with a 120$^{0}$ fiber orientation angle

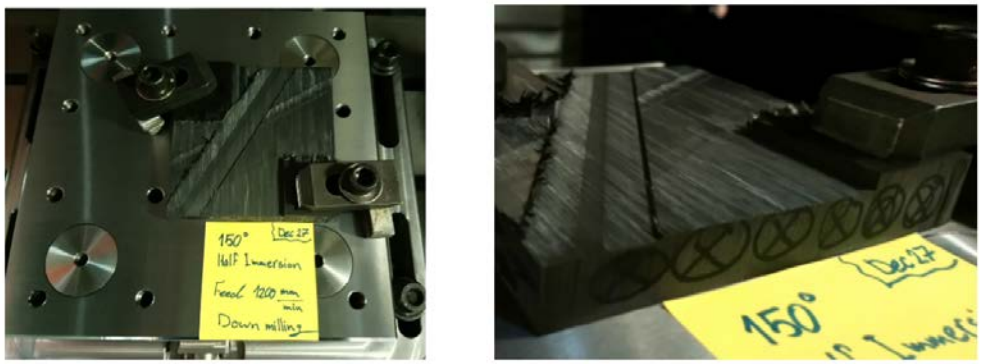


b) Half immersion down-milling with a 30$^{0}$ fiber orientation angle


c) Half immersion down-milling with a 120$^{0}$ fiber orientation angle

**Figure 5-8: Surface finishes affected by fiber orientation angle and machining condition**

### 5.1.4.2. General 2D Tool-path

In order to further investigate the performance of the mechanistic cutting force model, more complex tool paths are chosen for simulating the cutting forces in UD-CFRP. To verify this claim, in this study semi-circular tool-path millings were conducted as shown in Figure 5-9, with its machining parameters tabulated in Table 6.

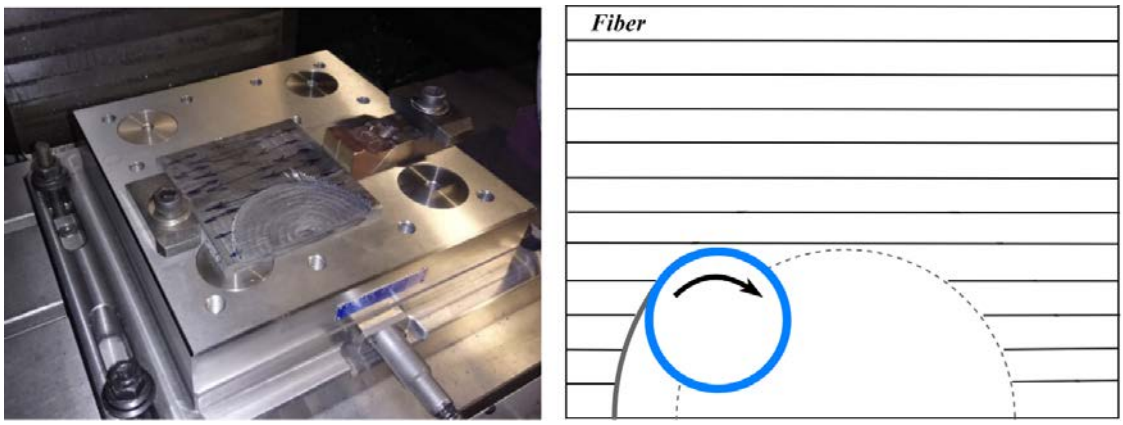


**Figure 5-9: Semi-circular tool path milling in UD-CFRP**

**Table 6: Machining condition for circular path milling**

| Machining Type | Chip Load (mm/rev/flute) | Spindle Speed (rpm) | Axial DOC (mm) | Radial DOC (mm) |
|---|---|---|---|---|
| **Up-milling** | 0.05 | 4000 | 1 | 5 |

Following is the G-Code used for this experiment:

```
%
G17 G40 G49 G80
G90 G00 G54 X0. Y0.
G91 G28 Z0.
G90 G54 G00 X14. Y-10.
M6 T1
G43 H01 Z5.
M3 S4000
G01 F100 Z-1.
F400 Y0.
G02 X104. Y0. I45. J0. F400
G01 F400 Y-10.
G91 G28 Z0.
M30
%
```

The reason for choosing this tool-path is that it enables one to calculate the changes of the angle between cutting direction and fiber orientation along the circle based on the chosen feed rate and the radius of the circular path using dexel or analytical calculations. Figure

5-10 shows the measured forces in dynamometer coordinates (X and Y directions) along the circular path.

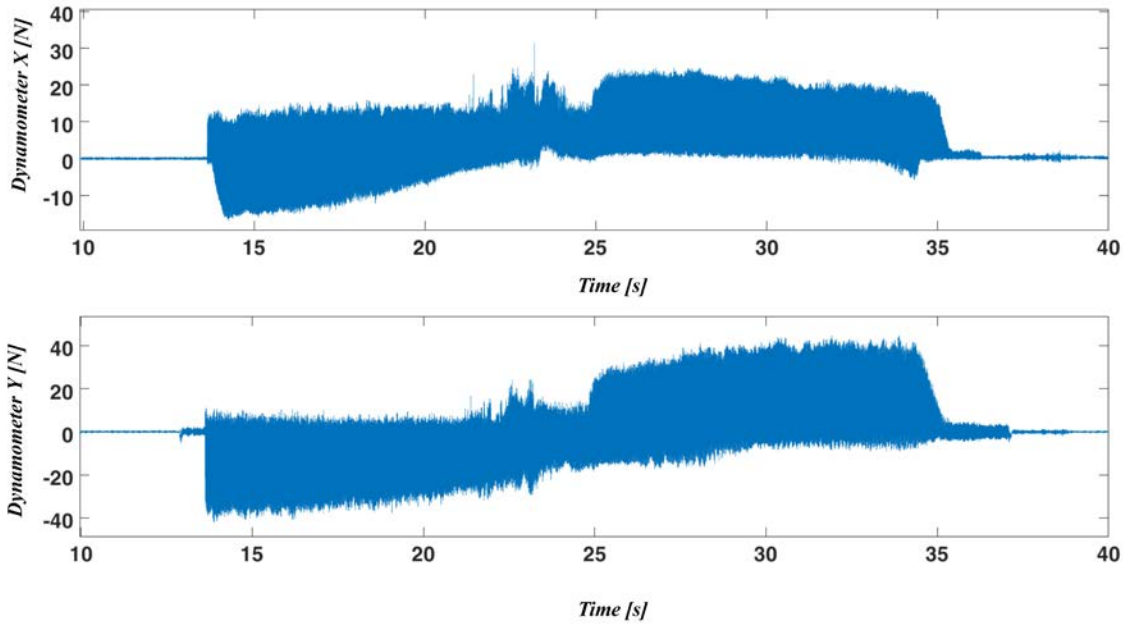


**Figure 5-10: measured forces along the circular path**

## 5.2. Data Analysis and Results

Cutting force measurements during UD-CFRP milling operations with fixed fiber angle orientations described in Section 5.1 are employed here to identify the cutting coefficients associated with up/down milling operations. The identified cutting coefficients are then employed to regenerate cutting forces in various cutting conditions including machining at fiber orientation angles that were not employed in the identification procedure.

In order to validate the proposed procedure in Chapter 4 that expands the cutting coefficients using a Fourier series expansion the identified coefficients are used to predict the cutting forces in a more complex semi-circular toolpath.

### 5.2.1. Cutting Constants Identification in Up-Milling

Measured cutting forces in half immersion up milling operations with three fiber orientation angles are used for the cutting coefficient calculation. These fiber angles are

90°, 120°, and 150°. Measured forces in the X and Y directions of the dynamometer were transformed into the feed and normal directions of machining. In each fiber cutting angle, the average normal and feed forces at measured chip loads are determined. It was observed, as expected, the average forces vary linearly with the changes in the chip loads. Therefore, average cutting forces as functions of chip loads at each fiber orientation are modeled using line fits. Figure 5-11 presents the fitted lines for the three fiber orientation angles of 90°, 120°, and 150°.

The average cutting forces are determined using the procedure developed in chapter 4. Establishing Eqn. (4.9) in three fiber orientation angles of 90°, 120°, and 150° with known coefficients $b_{ij}(\theta), i = 0,1, j = x, y$, the coefficients of the mechanistic cutting force model are obtained as presented in Table 7. For better visualization of the obtained results in Figure 5-12 the four cutting coefficients of $K_{tc}, K_{te}, K_{rc}$, and $K_{re}$ are plotted as a function of fiber cutting angle $\beta$.

**Table 7: Coefficients of mechanistic cutting force model (Up Milling)**

| | $K_{tc}(\beta)$ | $K_{te}(\beta)$ | $K_{rc}(\beta)$ | $K_{re}(\beta)$ |
|---|---|---|---|---|
| $K_0$ | 101.6334 | 9.4752 | 72.0094 | 14.3051 |
| $K_{1s}$ | -83.7773 | -5.2799 | -36.6482 | -10.3640 |
| $K_{1c}$ | 23.9211 | -4.1884 | 10.3248 | -6.2103 |

In a similar manner cutting constants may be obtained using experiments conducted on CFRPs with different orientation angles. Table 8 tabulates cutting forces obtained from CFRPs with orientation angles 30°, 60°, and 90° which lead to a non-physical mechanistic model due to disturbances in measured forces. The cause for the disturbances is discussed later in chapter 6.

**Table 8: Non-physical cutting force model (Up Milling)**

| | $K_{tc}(\beta)$ | $K_{te}(\beta)$ | $K_{rc}(\beta)$ | $K_{re}(\beta)$ |
|---|---|---|---|---|
| $K_0$ | 99.2176 | 15.2586 | 18.7037 | 13.1710 |
| $K_{1s}$ | -134.4890 | 4.2265 | -132.1553 | -14.9778 |
| $K_{1c}$ | -8.1790 | 1.6369 | -52.3032 | -4.5476 |

A physical cutting constant is positive real-valued therefore when it is expended using a single harmonic Fourier series the series constants must satisfy the following requirements:

$$K_0 > |K_{1s}|, K_0 > |K_{1c}| \tag{5.1}$$

As the series constant obtained for $K_{tc}(\beta)$, $K_{rc}(\beta)$, and $K_{re}(\beta)$ do not meet these requirements, these obtained cutting constants become negative-valued at some cutting angles and hence are not considered to be physically justifiable.

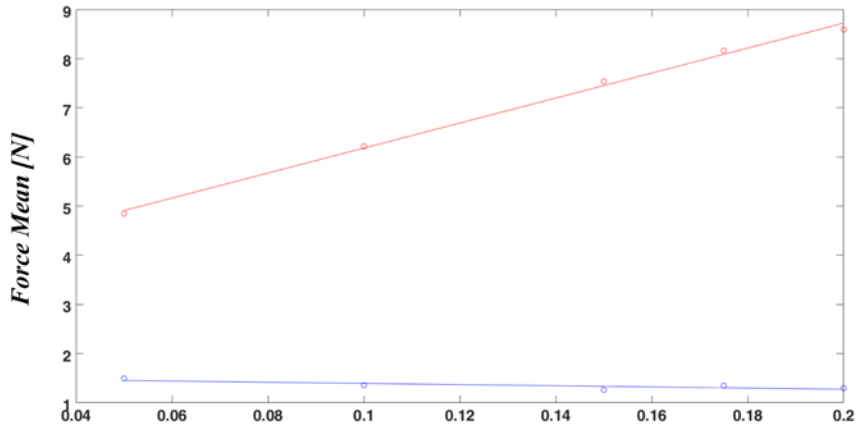


*a) Fiber orientation angle 150º*

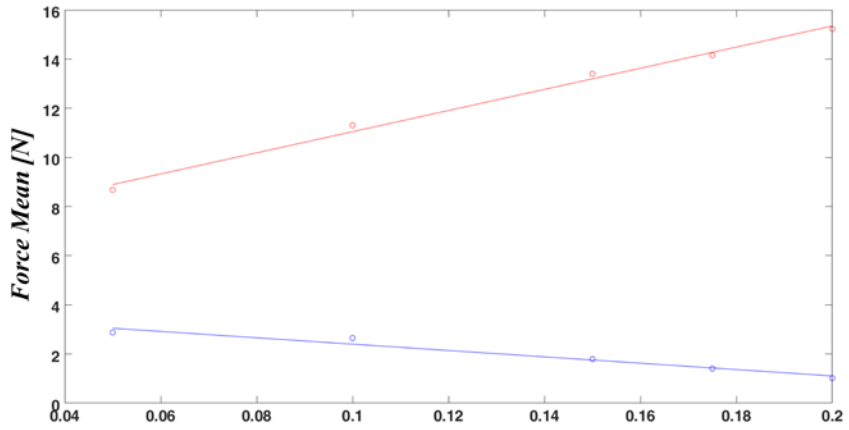


*b) Fiber orientation angle 120º*

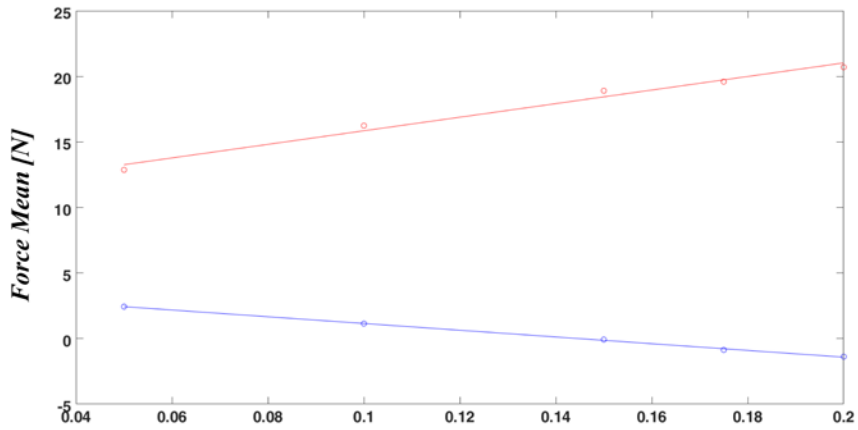


*c) Fiber orientation angle 90º*

**Figure 5-11: Average force, linear curve fitting result for a half immersion up milling cut at a spindle speed of 4000 rpm**

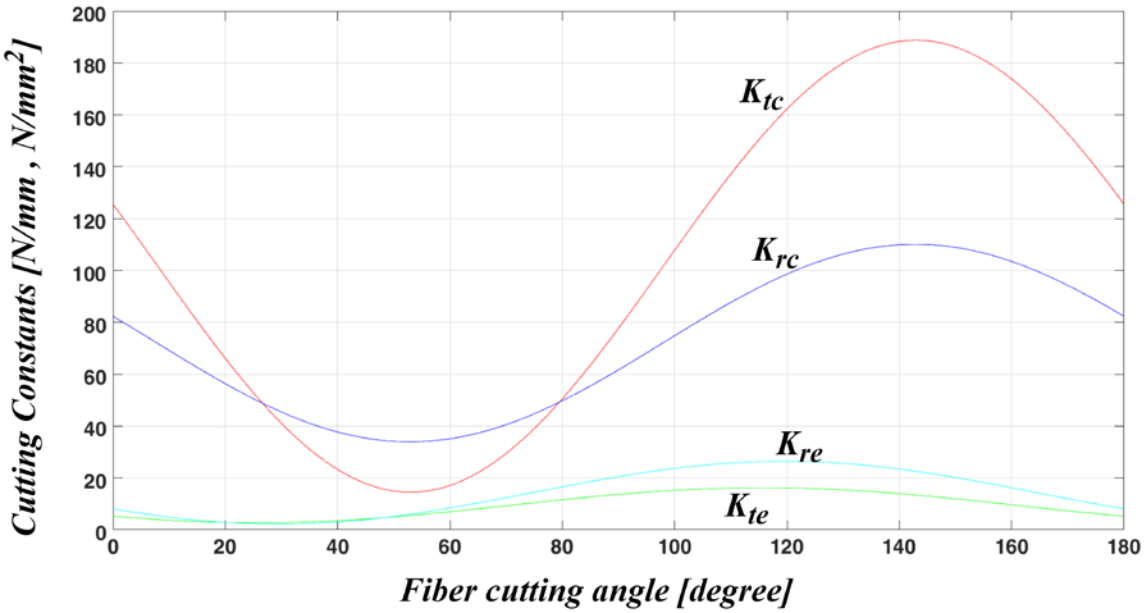


**Figure 5-12: Cutting force coefficients with fiber cutting angle for CFRP up-milling**

In order to verify the predictability of identified cutting force model, the cutting forces measured at orientation angles of 60$^o$, and 30$^o$ are regenerated via the coefficients tabulated in Table 7 as shown in Figure 5-13. The measured forces at these orientations are not employed in the identification of force coefficients and high correlations between measured and calculated shows that the cutting constants obtained from the experiments are accurate.

The accuracy of the identified mechanistic cutting force model is now verified and it may be used to predict cutting forces in any given tool path as will be demonstrated in the following sections of this chapter.

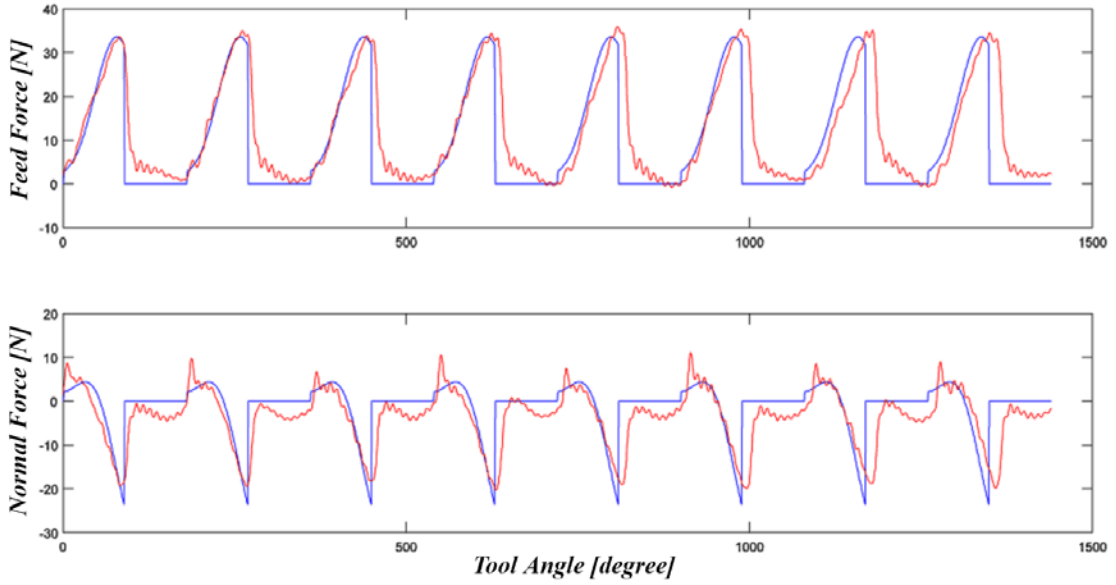


*a) Fiber orientation angle 30*

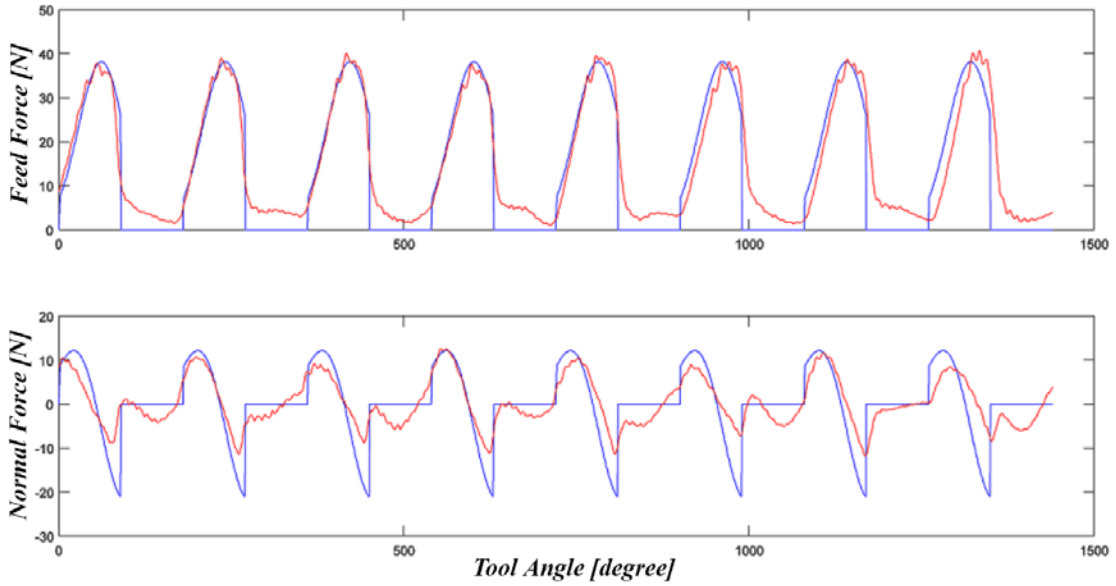


*b) Fiber orientation angle 60*

**Figure 5-13: Measured and simulated cutting forces for c= 0.05 mm/flute/rev at two different fiber orientation**

### 5.2.2. Cutting Constants Identification in Down-Milling

Similar to the previous section measured cutting forces in half immersion down milling operations with three fiber orientation angles are used for the cutting coefficient calculation. These fiber angles are 0º, 30º, and 60º. Again measured forces in the X and Y directions of the dynamometer were transformed into the feed and normal directions of machining. In each fiber orientation angle, the average normal and feed forces at measured chip loads are determined. It was observed, as expected, the average forces vary linearly with the changes in the chip loads. The average cutting forces as functions of chip loads at each fiber orientation are obtained using line fits. Figure 5-14 presents the fitted lines for the three fiber orientation angles of 0º, 30º, and 60º.

One obtains the coefficients of mechanistic cutting force model in down milling similar to those obtained in up milling. To visualize the obtained cutting coefficients, the four cutting coefficients of $K_{tc}, K_{te}, K_{rc}$, and $K_{re}$ are tabulated in Table 9 and are also plotted as a function of fiber cutting angle $\beta$ in Figure 5-15. Also, Figure 5-16 demonstrates the cutting forces measured at orientation angle 30º and associated forces regenerated via the coefficients shown in Table 9.

**Table 9: Coefficients of mechanistic cutting force model (Down Milling)**

| | $K_{tc}(\beta)$ | $K_{te}(\beta)$ | $K_{rc}(\beta)$ | $K_{re}(\beta)$ |
|---|---|---|---|---|
| $K_0$ | 185.2256 | 6.1987 | 51.8219 | 18.2583 |
| $K_{1s}$ | 7.1597 | -8.9324 | 5.4066 | -16.4038 |
| $K_{1c}$ | -64.1298 | 6.6684 | -10.3650 | -1.0891 |

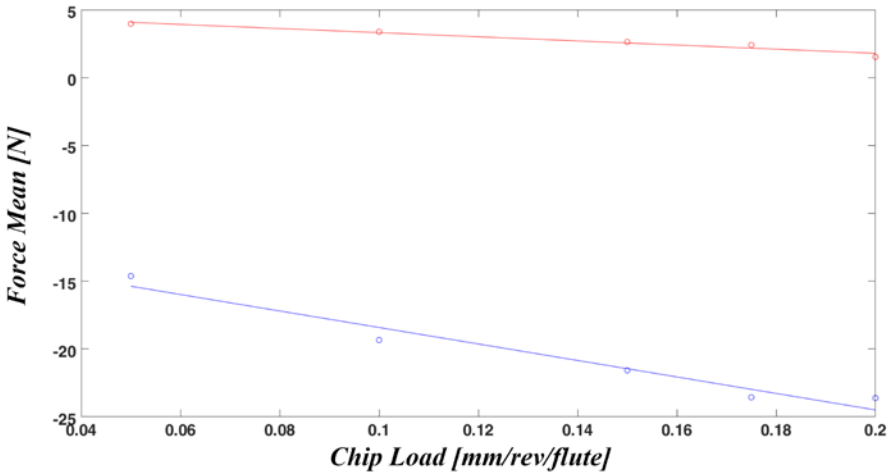


*a) Fiber orientation angle 0º*

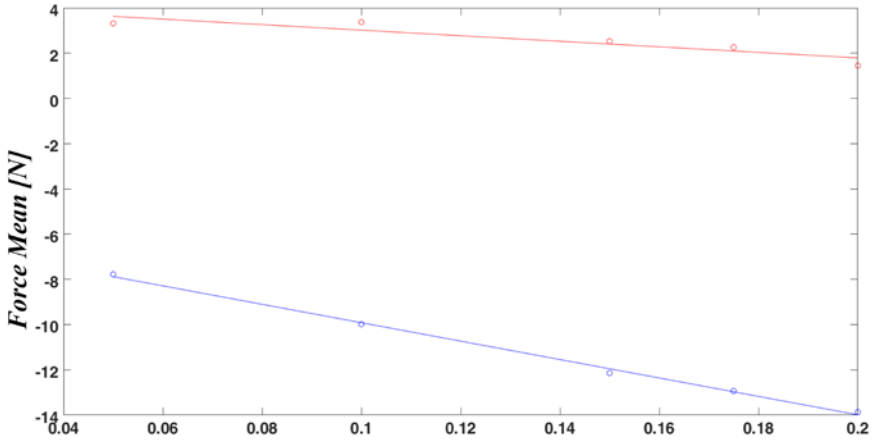


*b) Fiber orientation angle 60º*

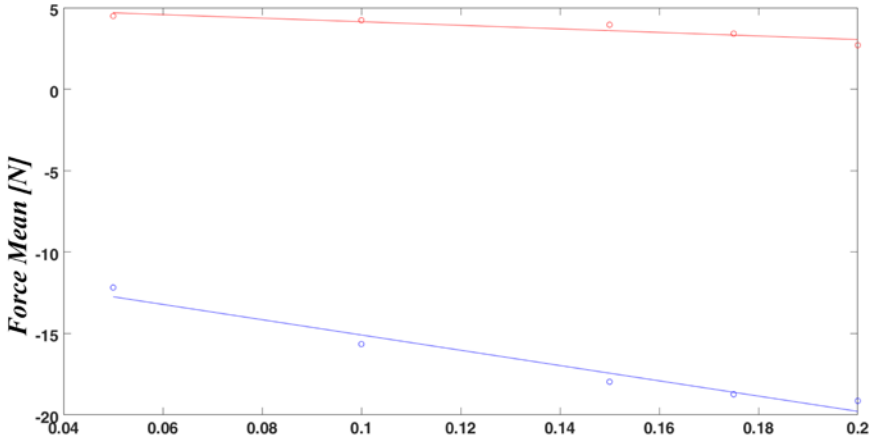


*c) Fiber orientation angle 30º*

**Figure 5-14: Average force, linear curve fitting result for a half immersion down milling cut at a spindle speed of 4000 rpm**

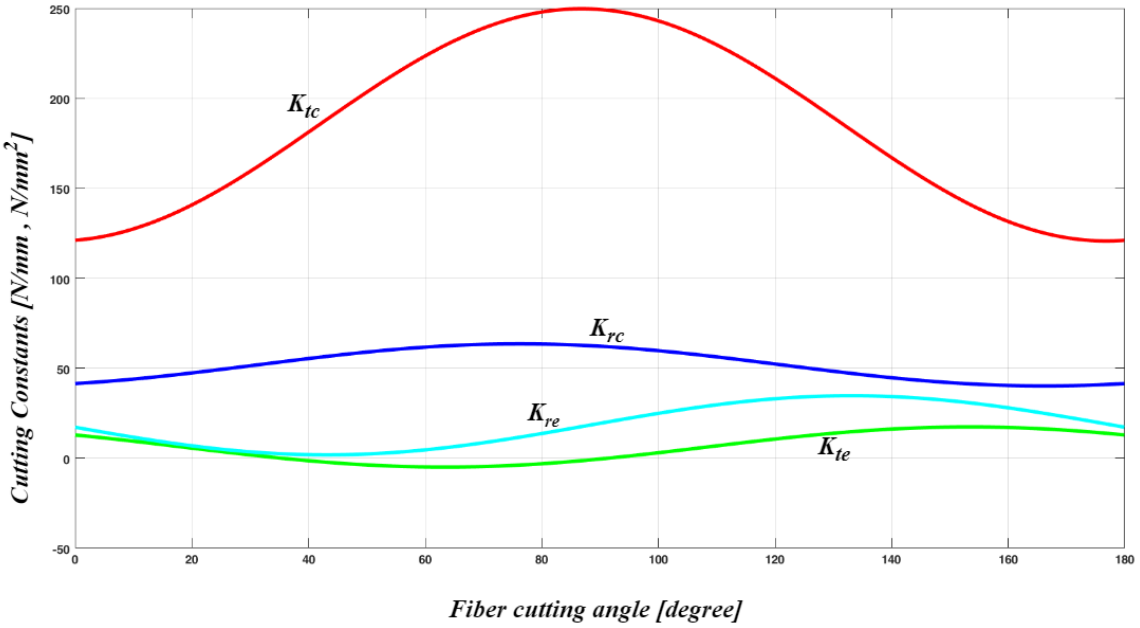


**Figure 5-15: Cutting force coefficients with fiber cutting angle for CFRP down-milling**

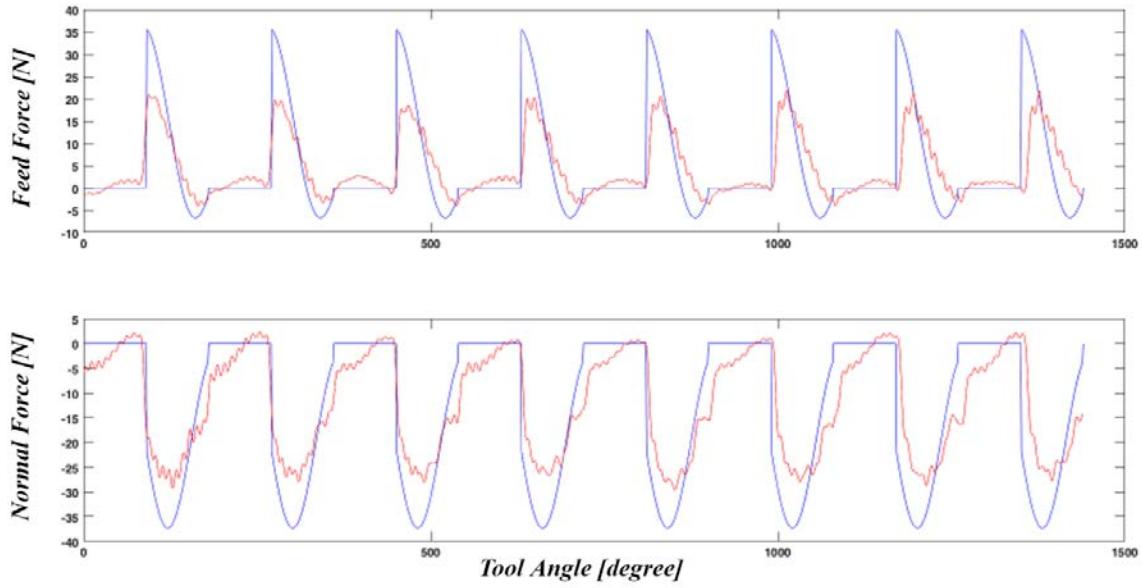


**Figure 5-16: Measured and simulated cutting forces for c= 0.05 mm/flute/rev at 30-degree fiber orientation**

Using the identified cutting coefficients in half-immersion down/up milling operations, it is possible to regenerate any complex 2D toolpath half-immersion milling forces. The

following section validates this claim by regenerating milling forces in a semi-circular path-way.

### 5.2.3. Semi-Circular Tool Path

With the mechanistic force model developed using UD-CRFP millings, in this section cutting forces are simulated for more complex tool paths. In this practice semi-circular tool-path half-immersion millings were conducted and resultant forces are compared to the regenerated forces using the presented mechanistic force model.

Figure 5-17 shows the calculated and measured forces in dynamometer coordinates (X and Y directions) along the circular path indicating accurate predictions obtained by the mechanistic force model.

The simulated force in X direction deviates from the measured force at the end of machining operations (during the time of 30 to 35 seconds). This is due to delamination accrued at the end of the circular path. At this position, the chip was not actually cut and lead to the deviation between measured and predicted forces at this location.

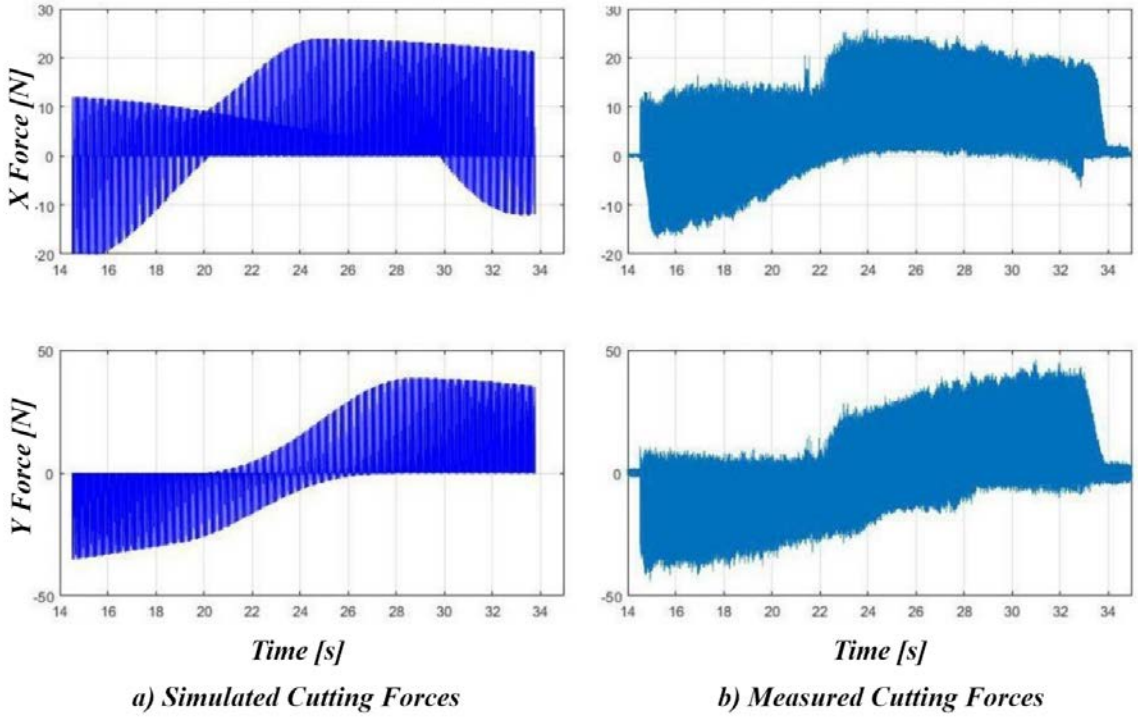


**Figure 5-17: Measured and simulated cutting forces along a circular path**

The consistency between measured and predicted forces validates the accuracy of presented mechanistic model in generating milling force.

# Chapter 6
# Discussion and Analysis

A mechanistic force model is presented in this research study and its predictions are validated against experimental observations. The focus of these discussions is to demonstrate more details regarding the mechanistic cutting force model of CFRP including its benefits and shortcomings.

## 6.1. Average Cutting Force Coefficients

The average cutting force coefficients are obtained in the previous chapter from measured cutting forces of UD-CFRP workpiece. It was noticed not all experimental results lead to acceptable force coefficients and the resultant coefficients in some cases may not be meaningful. In some fiber orientations after the tool passage, the uncut material was pushed out of the plane of the cut resulting "wisps" emerging from the work surface. As shown in Figure 6-1 a cut with low surface quality is achieved in these fiber orientations.


**Figure 6-1: Wisps emerging from the work surface**

The experiments conducted during the current study are listed in Table (6-1). Reasonable cutting constants are achieved from UD-CFRP milling operations with fiber orientation angles:

- 90, 120, and 150 degrees in up milling and,
- 0, 30, and 60 data sets in down milling.

In these fiber orientations, no residues or uncut material were observed and excellent cut quality was achieved on the workpiece.

The resultant cutting constants are able to regenerate milling forces for all experimental measurements cases even for those fiber orientations with poor surface quality. This due to the fact that uncut parts form a small fraction of chip load, and do not change the cutting force values significantly.

## 6.2. Regenerating Cutting Forces

In comparing the measured cutting forces and the regenerated ones obtained from the mechanistic model, such as the one shown in Figure 6-2, good correlations between these two sets of data are noticed. However, the existence of high harmonics in experimental results is noticeable which is not reflected in the mechanistic model force predictions.

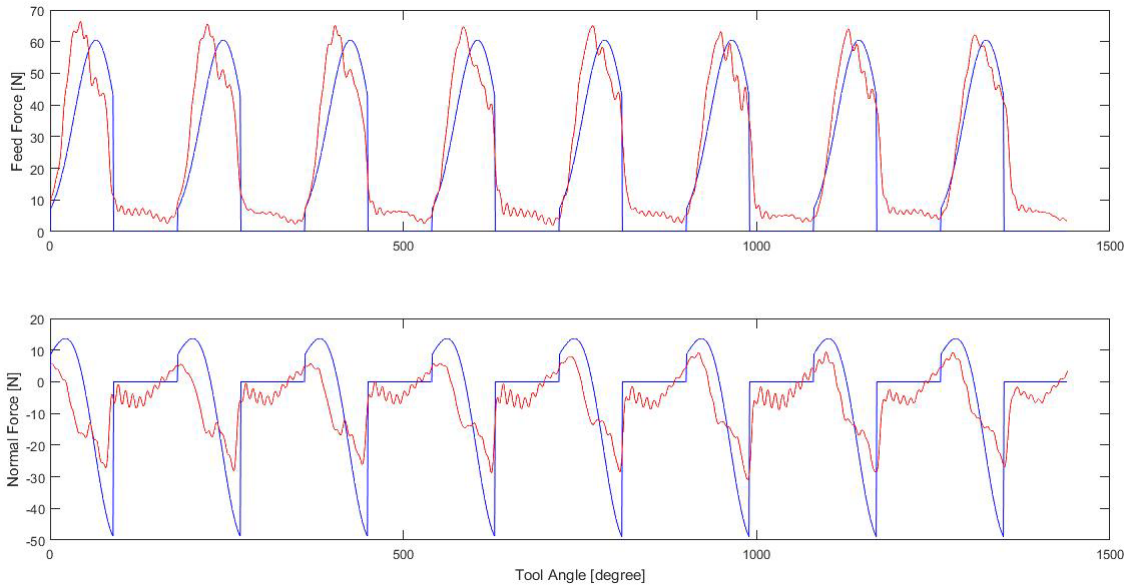


**Figure 6-2: Measured and regenerated forces in a UD-CFRP up-milling operation with a fiber orientation angle of $\theta = 60^o$ and $c = 0.20[mm/\ flute]$**

It may be assumed that the deviations between model predictions and experimental observations are partly related to the order of series which is selected to define the cutting force coefficients. In all reported force coefficients in this study, the Fourier series

expansion is defined using only one harmonics. This is due to the fact that single harmonic force coefficients were able to regenerate milling forces with sufficient accuracy. The question may arise whether it is possible to achieve more precise cutting force predictions by using extra harmonics in the series expansions of coefficients.

Figure 6-3 shows the identified cutting force constants obtained from up-milling experiments reported in chapter 5. These up-milling half immersion experiments were performed on UD-CFRPs with fiber orientation angles of 30°, 60°, 90°, 120°, and 150°. The Fourier series used in the identification contains two harmonics, i.e.

$$K_{mn}(\beta) = \sum_{i=0}^{2} K_{mn,ic}\cos(2i\beta) + K_{mn,is}\sin(2i\beta), m = t,r, n = c,e \qquad (6.1)$$

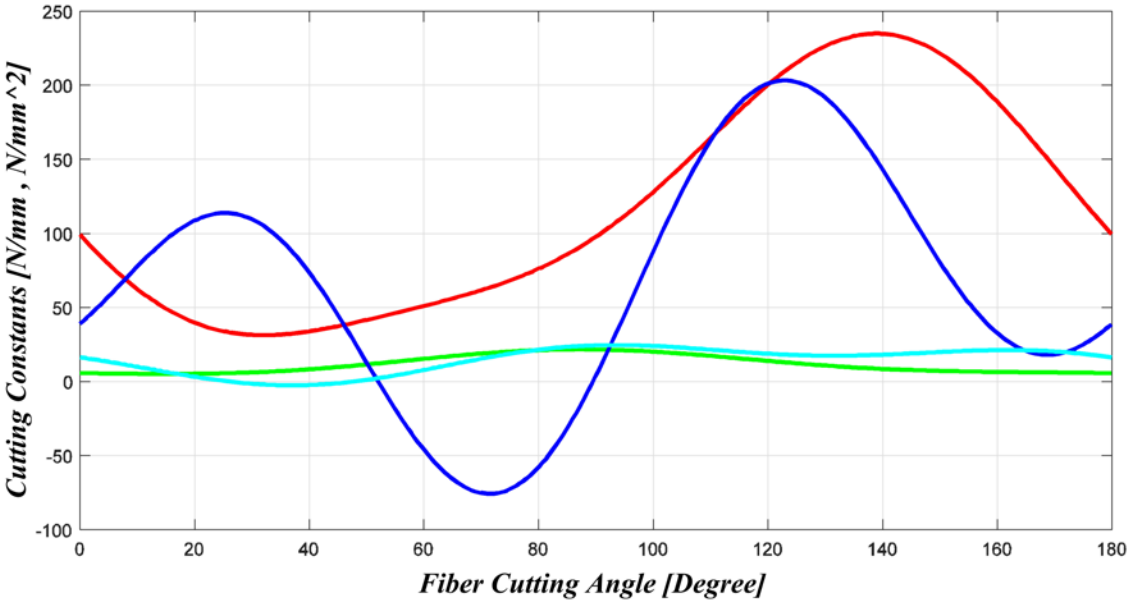


**Figure 6-3: Identified cutting constants ($K_{tc}$ (red), $K_{te}$(green), $K_{rc}$(blue), $K_{re}$(crayon))**

The identified force constants are tabulated in Table 10.

**Table 10: Identified cutting force constants**

| | $K_{tc}(\beta)$ | $K_{te}(\beta)$ | $K_{rc}(\beta)$ | $K_{re}(\beta)$ |
|---|---|---|---|---|
| $K_0$ | 116.9574 | 11.6898 | 64.7601 | 14.3328 |
| $K_{1s}$ | -97.9113 | 0.1281 | -62.9651 | -9.3318 |
| $K_{1c}$ | 0.7226 | -7.9538 | 17.5266 | -4.0694 |
| $K_{2s}$ | -11.7393 | -0.7095 | 79.7292 | -3.0359 |
| $K_{2c}$ | -18.4258 | 1.9867 | -43.1729 | 6.0833 |

As seen in Figure 6-3 the obtained cutting force coefficient $K_{rc}(\beta)$ is not physically justifiable. This is due to the fact that measured forces on fiber orientation angles of $30^o$, $60^o$ are influenced by uncut fibers emerging from the work surface.

It was not possible to obtain the contribution of higher Fourier series harmonics on the cutting constants using the available experimental data. However, it is possible to focus on the nature of the mechanistic force model to justify the observed deviations. The mechanistic cutting force model defines a static relation between the chip load and cutting forces and does not consider the machining dynamics. The measured forces contain harmonics related to spindle vibrations which are not considered in the mechanistic cutting force model.

## 6.3. Applying the Model to an Arbitrary Tool Path

In this study, a mechanistic force model is successfully applied to determine cutting forces in a semicircular tool path. In the previous chapter, it was reported that the measured cutting forces and regenerated forced determined by the corresponding mechanistic model are in excellent agreements. However, one should bear in mind such results can only be obtained using a number of carefully conducted experiments along with detailed processing of the test results.

One of the main steps in developing mechanistic cutting force model is to identify the average cutting force coefficients. A set of UD-CFRP milling experiments were conducted with various chip loads while keeping all other milling parameters such as:

- Immersion angles (start and end angels, up/down milling).
- Axial depth of cut, and
- Fiber orientation angle.

The experimentally obtained average cutting forces are then employed in the identification of cutting force constants.

The resultant mechanistic model provides accurate predictions of the cutting forces. However, if only one of the machining parameters is changed the identified model is no longer valid [29]. The extreme case dependency of cutting constants which limits its use is one of the mechanistic force model features which can be found in metal cuttings as well. Ref. [30] studies the variation of cutting constants in the milling of the aluminum workpiece under different machining conditions. The experimental study clearly demonstrates the cutting constants are changed when milling condition is varied from up-milling to down-milling or radial immersion percentage is changed.

Ref.[27] provides a mechanistic model for slot milling of CFRPs without considering the effect of up/down milling in cutting forces. However, it clearly states: “The radial cutting force coefficients calculated at $135^{o}$ fiber cutting angle are quite different from each other. This implies that upon reaching $135^{o}$ fiber cutting angle the direction of milling influences cutting forces.”

In the semicircular path milling experiments, half immersion up milling machining was conducted. If one changes the machining condition from up to down milling the cutting forces would naturally change and one needs to use corresponding cutting constants. As seen in Chapter 5 the cutting constants vary from up to down milling drastically.

## 6.4. Conclusion

A mechanistic CFRP cutting force model that considers variations of chip formation mechanism in various fiber cutting angles is presented in this thesis. The cutting force coefficients are assumed to be periodic with respect to the fiber cutting angle. A new method is presented to identify the periodic cutting force coefficients based on the average milling forces measured during milling UD composite layers. The accuracy of the presented model and the identification approach are verified by comparing the simulated milling forces against the measured ones.

The presented method provides a practical approach for calibrating mechanistic cutting force models in various combinations of tools and composite materials; however, unavoidable characteristics of CFRP milling processes such as excessive tool wear and fiber pull-out will influence the accuracy of the model predictions. Studying the relations between variations of the cutting force coefficients and the physics of chip formation at different fiber cutting angles may provide a better understanding of the mechanics of the process.

# References

[1] R. Fabian, “Fundamentals of carbon Fibre Reinforced Polymer (CFRP) Machining,” ETH ZURICH, 2017.

[2] J. Fleischer, R. Teti, G. Lanza, and P. Tarisai, “Composite Materials Parts Manufacturing,” *CIRP Ann. Manuf. Technol.*, vol. 67, no. 2, pp. 603–626, 2018.

[3] D. Che, I. Saxena, P. Hhan, and P. Guo, “Machining of Carbon Fiber Reinforced Plastics / Polymers : A Literature Review,” *J. Manuf. Sci. Eng*, vol. 136, no. 3, pp. 1–22, 2014.

[4] V. Lopresto, A. Caggiano, and R. Teti, “High Performance Cutting of Fibre Reinforced Plastic Composite Materials,” *Procedia CIRP*, vol. 46, pp. 71–82, 2016.

[5] P. Ghidossi, M. El Mansori, and F. Pierron, “Edge machining effects on the failure of polymer matrix composite coupons,” *Compos. Part A*, vol. 35, no. 7–8, pp. 989–999, 2004.

[6] A. Koplev, A. Lystrup, and T. Vorm, “The cutting process , chips , and cutting forces in machining CFRP,” *Composites*, vol. 14, no. 4, pp. 371–376, 1983.

[7] L. Lasri, M. Nouari, and M. El Mansori, “Modelling of chip separation in machining unidirectional FRP composites by stiffness degradation concept,” *Compos. Sci. Technol.*, vol. 69, no. 5, pp. 684–692, 2009.

[8] D. H. Wang, M. Ramulu, and D. Arola, “Orthogonal Cutting Mechanisms of Graohite/Epoxy Composite. Part I: Unidirectional Laminate,” *Int. J. Mach. Tools Manufact.*, vol. 35, no. 12, pp. 1623–1638, 1995.

[9] M. Ramulu, “Machining and surface integrity of fibre-reinforced plastic

composites," *Sadhana*, vol. 22, no. 3, pp. 449–472, 1997.

[10] D. Arola, M. Ramulu, and D. H. Wang, "Chip formation in orthogonal trimming of graphite / epoxy composite," *Compos. Part A*, vol. 27, no. 2, pp. 121–133, 1996.

[11] X. M. Wang and L. C. Zhang, "An experimental investigation into the orthogonal cutting of unidirectional fibre reinforced plastics," *Int. J. Mach. Tools Manufact.*, vol. 43, pp. 1015–1022, 2003.

[12] M. Ramulu, C. W. Wern, and J. L. Garbini, "Effect of Fibre Direction on Surface Roughness Measurements of Machined Graphite / Epoxy Composite," *Compos. Manuf.*, vol. 4, no. 1, pp. 39–51, 1993.

[13] D. Nayak, N. Bhatnagar, and P. Mahajan, "MACHINING STUDIES OF UD-FRP COMPOSITES PART 2 : FINITE ELEMENT ANALYSIS," *Mach. Sci. Technol.*, vol. 9, no. 4, pp. 503–528, 2007.

[14] M. Mahdi and L. Zhang, "An adaptive three-dimensional finite element algorithm for the orthogonal cutting of composite materials," *J. Mater. Process. Technol.*, vol. 113, no. 1–3, pp. 368–372, 2001.

[15] M. Mahdi and L. Zhang, "A finite element model for the orthogonal cutting of fiber-reinforced composite materials," *J. Mater. Process. Technol.*, vol. 113, no. 1–3, pp. 373–377, 2001.

[16] D. Arola, M. B. Sultan, and M. Ramula, "Finite Element Modeling of Edge Trimming Fiber Reinforced Plastics," *J. Manuf. Sci. Eng*, vol. 124, no. 1, pp. 32–41, 2000.

[17] H. Hocheng, H. Y. Puw, and Y. Huang, "Preliminary study on milling of unidirectional carbon fibre-reinforced plastics," *Compos. Manuf.*, vol. 4, no. 2, pp.

103–108, 1993.

[18] D. Kalla, J. Sheikh-ahmad, and J. Twomey, “Prediction of cutting forces in helical end milling fiber reinforced polymers,” *Int. J. Mach. Tools Manuf.*, vol. 50, no. 10, pp. 882–891, 2010.

[19] B. Denkena, D. Boehnke, and J. H. Dege, “Helical milling of CFRP – titanium layer compounds,” *CIRP J. Manuf. Sci. Technol.*, vol. 1, pp. 64–69, 2008.

[20] E. Uhlmann, F. Protz, B. Stawiszynski, and S. Heidler, “Ultrasonic assisted milling of reinforced plastics,” *Procedia CIRP*, vol. 66, pp. 164–168, 2017.

[21] I. Sultana, Z. Shi, H. Attia, and V. Thomson, “A new hybrid oscillatory orbital process for drilling of composites using superabrasive diamond tools,” *CIRP Ann. - Manuf. Technol.*, vol. 65, no. 1, pp. 141–144, 2016.

[22] K. Szallies, N. Siebert, and J. Pierre, “Low frequency oscillated milling of carbon fiber-reinforced plastics,” *Procedia CIRP*, vol. 66, pp. 153–158, 2017.

[23] W. Hintze, D. Hartmann, and C. Schütte, “Occurrence and propagation of delamination during the machining of carbon fibre reinforced plastics ( CFRPs ) – An experimental study,” *Compos. Sci. Technol.*, vol. 71, no. 15, pp. 1719–1726, 2011.

[24] W. Hintze and D. Hartmann, “Modeling of delamination during milling of unidirectional CFRP,” *Procedia CIRP*, vol. 8, pp. 444–449, 2013.

[25] E. Uhlmann, F. Sammler, S. Richarz, G. Reucher, R. Hufschmied, and A. Frank, “Machining of carbon and glass fibre reinforced composites,” vol. 46, pp. 63–66, 2016.

[26] M. Henerichs, R. Voß, F. Kuster, and K. Wegener, “Machining of carbon fiber

reinforced plastics : Influence of tool geometry and fiber orientation on the machining forces," *CIRP J. Manuf. Sci. Technol.*, vol. 9, pp. 136–145, 2015.

[27] Y. Karpat, O. Bahtiyar, and B. Deger, "Mechanistic force modeling for milling of unidirectional carbon fiber reinforced polymer laminates," *Int. J. Mach. Tools Manuf.*, vol. 56, pp. 79–93, 2012.

[28] N. Duboust *et al.*, "2D and 3D Finite Element models for the edge trimming of CFRP," *Procedia CIRPCIRP*, vol. 58, pp. 233–238, 2017.

[29] Y. Altintas, *Manufacturing Automation: Metal Cutting Mechanics, Machine Tool Vibrations, and CNC Design*, 2nd ed. Cambridge University Press, 2012.

[30] M. A. Rubeo and T. L. Schmitz, "Milling Force Modeling : A Comparison of Two Approaches," *Procedia Manuf.*, vol. 5, pp. 90–105, 2016.

[31] MAL Manufacturing Automation Laboratories Inc., "CutPro 11 - User Manual," 2016.

[32] S. Luo, R. Bayesteh, Z. Dong, and M. B. G. Jun, "3-Axis Milling Simulation for Carbon Fiber Reinforced Polymer ( CFRP ) Composites," 한국정밀공학회지, vol. 33, no. 6, pp. 447–452, 2016.

[33] S. Luo, Z. Dong, and M. B. G. Jun, "Optimal tool orientation generation and chip volume / cutting force predictions for 5-axis CNC machining of curved surfaces using flat-end mills," *Comput. Aided. Des. Appl.*, vol. 4360, pp. 331–342, 2017.

[34] E. Abele, J. Bauer, M. Pischan, O. Stryk, M. Friedmann, and T. Hemker, "Prediction of the tool displacement for robot milling applications using coupled models of an industrial robot and removal simulation," in *CIRP 2nd Inter Conf on Process Machine Interactions*, 2010.

[35] M. Farhadmanesh, A. S. Salehi, K. Ahmadi, and M. B. G. Jun, “Virtual milling of Fibre Reinforced Polymers,” in *6th International Conference on Virtual Machining Process Technology*, 2017, pp. 1–6.

[36] D. Wang, M. Ramulu, and D. Arola, “Orthogonal Cutting Mechanisms of Graphite/Epoxy Composite. Part II: Multi-Directional Laminate,” *Int. J. Mach. Tools Manufact.*, vol. 35, no. 12, pp. 1639–1648, 1995.

[37] OSG Tool Corporation, “OSG Milling Tools Catalogue,” Japan, 2018.

[38] KISTLER Instrument Corp., “Multicomponent Dynamometer 9255 C Catalogue,” 2012.

[39] KISTLER Instrument Corp., “3-Component Dynamometer 9255 C Instruction Manual,” 2015.

[40] Amana Tool Corporation, “Carbon Fiber Panel CNC Cutting Speed and Feed Chart,” 2015.